UNIVERSIDADE DE LISBOA

FACULDADE DE CIÊNCIAS

DEPARTAMENTO DE FÍSICA

Development of carriers for insulin delivery for wound healing applications

Francisca Ribeiro Mendes

Mestrado Integrado em Engenharia Biomédica e Biofísica

Perfil em Engenharia Clínica e Instrumentação Médica

Dissertação orientada por:

Prof. Pedro Ricardo Martins Lopes da Fonte

Prof. Hugo Alexandre Teixeira Duarte Ferreira

2021

Preface

The work contained in this Master dissertation was performed at the Institute for Bioengineering and Biosciences (iBB), Instituto Superior Técnico (Lisbon, Portugal), under the supervision of Professor Pedro Fonte and advisership of Prof. Ana Macedo. The developed project was performed in the framework of the project POCI-01-0145-FEDER-032610—PTDC/MEC-DER/32610/2017. funded by *FEDER - Fundo Europeu de Desenvolvimento* Regional funds through the COMPETE 2020 - Operational Programme for Competitiveness and Internationalization (POCI), and by Portuguese funds through *FCT - Fundação para a Ciência e a Tecnologia (FCT*), Portugal.

In the development of this work, it was achieved the publication of the following papers:

1. Ana S. Macedo, **Francisca Mendes**, Patrícia Filipe, Salette Reis, Pedro Fonte, Nanocarrier-Mediated Topical Insulin Delivery for Wound Healing, Materials, 14(15), 4257 (2021)

2. Melanie Pichlsberger, Urška Dragin Jerman, Hristina Obradović, Larisa Tratnjek, Pedro Fonte, Anja Hoegler, Monika Sundl, Julia Fuchs, Ana Sofia Macedo, **Francisca Mendes**, Andreina Schoeberlein, Mateja Erdani Kreft, Slavko Mojsilović, Ingrid Lang-Olip, Systematic review on the application of perinatal derivatives in animal models of cutaneous wound healing, Frontiers in Bioengineering and Biotechnology, 9:742858 (2021).

The work was also disseminated in the following international scientific conferences:

1. **Francisca Mendes**, Ana S. Macedo, Pedro Fonte, Co-encapsulation of mesenchymal stem cells and growth factors by microfluidics for wound healing applications, EuroNanoForum online conference, 2021. *Poster presentation*

2. **Francisca Mendes**, Vânia Silvério, Ana S. Macedo, Pedro Fonte, Co-encapsulation of mesenchymal stem cells and insulin for wound healing, NanoPT online conference, 2021. *Poster presentation*

Acknowledgements

I want to express my gratitude to all the people who supported me during these five years, without whom the conclusion of this work would not be possible.

Firstly, I would like to acknowledge to Professor Pedro Fonte for giving me the opportunity to join his group and for the trust he put in me. Also, for all the enthusiastic guidance and availability to help and teach me. This work would not be possible without him, and I am truly grateful for everything I learned at the lab in the last few months.

To Professor Hugo Ferreira for the availability to be my supervisor and for helping me.

To Professor Ana Macedo, I want to express my gratitude for the availability to help and for the willingness to listen to me. She is also acknowledged for all the support, advice, and conversations during these months.

I also want to thank to Professor Vânia Silvério for all the help in the microfluidics assays and for allowing the use of the INESC MN facilities.

To all the team at iBB of Instituto Superior Técnico, I want to leave my sincere thank you for the friendliness and for the great work atmosphere. A special thanks to my laboratory colleague João Prata, who always helped me in the way he could, for the companionship and for all the great spent moments.

To my sweet and loyal companion, Luna, my thanks for the friendship and for being a constant source of love.

To my beloved family, thank you for all the love and support. A special acknowledgment goes to my sisters-in-law for all the caring and emotional support. To my grandfather, wherever you are, thank you for having my back. You are always in my mind and heart.

To my mother, father, and brother, thank you for sharing my accomplishments with such great enthusiasm. A special acknowledgement goes to my parents for all the support, for believing in me, and for teaching me that I could be whatever I want. You taught me the most important values that I will always carry with me. This work would not be possible without you. To my brother, thank you for teaching me that happiness can be found in the little things. I'm deeply grateful for all the moments we spent together and for having you in my life.

Last but not least, I want to thank Hugo for always being present for me, in the good times and even more in the bad ones. Thank you for all the love, encouragement, and patience. During these 5 years you have been lifting me up and I would choose you another 100 times to come along in this journey with me.

Resumo

A prevalência de feridas crónicas representa um dos maiores problemas de saúde pública a nível global, em função dos longos períodos de cicatrização associados a tratamentos pouco eficazes. A cicatrização de feridas é um processo fisiológico dinâmico e organizado que permite a recuperação da integridade da pele após uma lesão. Assim, a interrupção deste processo está associada a um impacto negativo e significante na qualidade de vida dos pacientes. Pacientes com patologias como a diabetes e obesidade estão mais sujeitos ao aparecimento deste tipo de feridas, devido a condições inerentes de hiperglicemia e complicações cardiovasculares. A idade é também um fator de risco para este tipo de lesão. Ao longo das últimas décadas equipas de investigação têm-se dedicado à descoberta de novas terapias, sendo que a principal abordagem para este tipo de patologia consiste em eliminar o foco de inflamação e aplicar topicamente fatores de crescimentos exógenos. A insulina é um fator de crescimento com um preço reduzido e vastamente disponível no mercado, capaz de estimular a migração celular, acelerando o processo de cicatrização. Contudo, a eficácia da administração tópica de insulina torna-se reduzida devido à ação das protéases presentes no leito da ferida. Assim, torna-se fundamental desenvolver novos métodos eficazes e capazes de contrariar este efeito proteolítico, protegendo o fator de crescimento da degradação. A encapsulação da insulina em micropartículas é capaz de conferir estabilidade à proteína quando administrada na ferida, promovendo uma libertação controlada e uma maior adesão às superfícies mucosas. Estudos revelaram, também, que a administração tópica de células estaminais mesenquimais acelera o processo de cicatrização, promovendo a formação de novos vasos sanguíneos num processo designado angiogénese, e reduzindo a inflamação. Este tipo de células estaminais têm a capacidade de se autorrenovarem em diferentes linhagens celulares, secretar fatores de crescimento e outras biomoléculas. Para além disso, o secretoma destas células é capaz de promover a deposição de matriz extracelular e aumentar a estabilidade dos fatores de crescimento no leito da ferida. Por outro lado, os fatores de crescimento têm, também, influência ao nível da modulação do efeito destas células estaminais. Assim, a co-encapsulação de insulina em conjunto com células estaminais mesenquimais em micropartículas pode ser uma estratégia inovadora no campo da medicina regenerativa, com aplicação na regeneração de feridas crónicas. Relativamente à administração destes fatores terapêuticas, esta pode ser feita através de aplicação de hidrogéis, capazes de conferir proteção contra a degradação provocada pelo ambiente. O PVA é um polímero sintético solúvel em água frequentemente utilizado na produção de hidrogéis, que pode ser reticulado de modo a adquirir excelentes propriedades viscoelásticas. Os hidrogéis compostos por este polímero conferem à pele uma camada resistente ao stress provocado pelo processo de cicatrização, promovendo uma sensação de conforto quando são aplicados na ferida. Por outro lado, o alginato é um polímero natural conhecido pela sua capacidade de absorver os fluídos em excesso existentes nas feridas, mantendo a hidratação da pele. Também a glicerina é frequentemente utilizada em hidrogéis, funcionado como emoliente e conferindo estrutura ao mesmo. Assim, o primeiro objetivo deste trabalho é desenvolver um hidrogel com nanopartículas contendo insulina, através de ciclos de congelação-descongelação. Posteriormente, é necessário otimizar este hidrogel que deverá ser apto para aplicação tópica, promovendo uma sensação de conforto quando aplicado na ferida. Para isso, as suas propriedades reológicas, tais como a viscosidade, vão ser avaliadas de modo a garantir a obtenção de um sistema de administração de insulina apto para aplicação em feridas crónicas. Para proceder à caracterização e produção deste hidrogel foram utilizadas nanopartículas revestidas com quitosano previamente produzidas pelo grupo de investigação que foram depois incorporadas no hidrogel composto por PVA, alginato e glicerina. Note-se que as nanopartículas revestidas com quitosano foram apenas utilizadas para estudar as propriedades reológicas do hidrogel, de modo a otimizar a sua formulação. Nesta primeira fase foi possível estudar e compreender a influência das variáveis independentes (percentagem de quitosano, alginato e glicerina, e número de ciclos de congelação-descongelação) nas propriedades do sistema composto pelo hidrogel e nanopartículas. A variável com maior impacto

sobre as características do hidrogel é a quantidade de alginato, que influencia propriedades como a viscosidade e o potencial zeta. Correlacionando estes fatores tornou-se, então, possível, determinar a formulação ideal para o hidrogel. Numa segunda fase do projeto, pretende-se desenvolver um sistema para co-encapsulação de insulina com células estaminais mesenquimais através da técnica de microfluídica. Neste caso, o objetivo é estudar a estrutura da insulina após encapsulação, para mais tarde adicionar à formulação as células estaminais mesenquimais. A microfluídica foi a técnica escolhida para este efeito, uma vez que permite uma rápida produção de micropartículas com um tamanho e forma bem definidos, bem como a encapsulação de células em simultâneo. Assim, produziu-se um microchip com uma estrutura em forma de "T" e utilizaram-se propulsores de seringas para administrar duas fases imiscíveis com um fluxo constante. A fase contínua corresponde a uma solução de alginato e insulina, enquanto a fase dispersa corresponde a uma solução lipídica auto-emulsionante. Neste contexto, as partículas produzidas têm dimensões entre 10-100 µm, pelo que são consideradas micropartículas. Com o objetivo de otimizar a produção de micropartículas, produziram-se microchips com entradas e saídas reforçados para evitar pequenas fugas de conteúdo provocadas pela textura oleosa da fase dispersa. Apesar de eficaz, a técnica de microfluídica é bastante minuciosa, na medida em que é necessário determinar os fluxos ideias para um cada dos fluídos, possibilitando a formação de partículas esféricas. Para efeitos de controlo, foram produzidas partículas com e sem insulina. Uma vez produzidas, as partículas foram congeladas e posteriormente liofilizadas, com e sem crioprotetor. A morfologia da superfície das micropartículas foi avaliada através da técnica de microscopia eletrónica de varredura, e foram também realizados ensaio de libertação durante um período de 48 horas para avaliar e eficácia do sistema. A insulina foi depois extraída das micropartículas e a sua estrutura foi avaliada por microscopia de fluorescência, dicroísmo circular, espetroscopia de infravermelho com transformada de Fourier, e ensaios de Tio Flavina-T. Os resultados obtidos com o ensaio de libertação revelaram uma libertação uniforme e controlada de insulina durante as 48 horas, permitindo concluir que esta libertação poderá manter-se mesmo após este período. Os resultados de dicroísmo circular e microscopia de fluorescência revelaram que a insulina manteve a sua estrutura após encapsulação, com presença de apenas pequenas alterações. Os resultados de espetroscopia de infravermelho com transformada de Fourier confirmaram que a estrutura da insulina foi conservada após encapsulação, e não foram detetadas novas interações da proteína com o alginato. Os resultados obtidos relativamente às partículas congeladas com e sem crioprotetor revelaram-se semelhantes, sem grandes diferenças a notar relativamente a esta variável. Os resultados obtidos com este trabalho sugerem que a insulina pode ser eficazmente encapsulada através da técnica de microfluídica. Assim, reúnem-se condições para aliar os resultados obtidos em ambas as etapas deste trabalho, sendo que o produto final seria um hidrogel cuja formulação foi otimizada, contendo micropartículas com insulina, obtidas com recurso à técnica de microfluídica. Futuramente, pretende-se desenvolver um microchip com maior complexidade que permita encapsular as células estaminais mesenquimais em simultâneo com a insulina. Assim, será possível avaliar a viabilidade das células após encapsulação, bem como estudar a citotoxicidade e bioatividade da formulação *in vitro*. O resultado final será uma plataforma multipotente para administração tópica de fatores de crescimentos células estaminais mesenquimais para a cicatrização de feridas crónicas.

Palavras-chave: Cicatrização de feridas; Insulina; Feridas crónicas; Microfluídica; Hidrogel.

Abstract

The prevalence of chronic wounds is a challenging public health issue, due to long-time recovery and inefficacious treatments. Incidence of chronic wounds increase with age and pathologies such as diabetes and obesity are risk-factors. Insulin, a peptide hormone, is one of the cheapest growth factors available, being able to mitigate the compromised skin by triggering cell migration and proliferation, stimulating wound healing. Mesenchymal stem cells offer promising approaches for cell therapy because of their self-renewal capacities and multi-lineage differentiation. Besides, it was demonstrated that the presence of insulin improves MSCs function and survival, accelerating chronic wound healing. The co-encapsulation of mesenchymal stem cells and insulin in microparticles improves its stability in the wound area, provide adhesion to the mucosal surfaces, and preserve the sustained release. Therefore, this work started with the development and optimization of a hydrogel containing nanoparticles for topical insulin administration by freeze-thawing. The objective is to obtain a hydrogel with good rheological particles suitable for topical application. The second phase of the work consists of the development of a delivery system co-encapsulating insulin and mesenchymal stem cells by microfluidics. In this case, the aim is to evaluate the protein structure upon encapsulation to later encapsulate the stem cells. Microfluidics was the chosen technique for microparticle production because it allows the rapid generation of controlled size particles and simultaneous cell encapsulation. Once produced, microparticles were lyophilized with and without cryoprotectant. The surface morphology of the produced microparticles was evaluated using scanning electronic microscopy and the release profile of insulin was also evaluated. Insulin structure upon encapsulation was assessed by fluorescence microscopy, circular dichroism, Fourier transform infrared spectroscopy and thioflavin-T assay. The results obtained with circular dichroism, fluorescence microscopy, and thioflavin-T assay revealed that insulin structure was maintained upon encapsulation with minimal structural modifications. Moreover, the presence of cryoprotectant did not affect the results concerning insulin structure. Fourier transform infrared spectroscopy results showed confirm these results, and no interactions with alginate are evidenced. Finally, the results regarding the release profile of insulin revealed a sustained release during a period of 48 hours. The results obtained in both phases of this work suggest that the developed encapsulation technique can be applied to the production of microparticles co-encapsulating insulin and mesenchymal stem cells. Therefore, the next step consists of evaluate the mesenchymal stem cells viability upon encapsulation, and the cytotoxicity profile of the formulation, as well its bioactivity. Then, these microparticles can be incorporated into the optimized hydrogel, creating a delivery system suitable for topical administration, with wound healing applications.

Keywords: Wound Healing; Insulin; Chronic Wound; Microfluidics; Hydrogel.

Table of Contents

Resumo v
Abstract vii
List of Figures x
List of Tables xii
List of abbreviations and acronyms xiii
1. Introduction 1
1.1. Anatomophysiology of the skin 1
1.2. Wound Healing 3
1.2.1. Normal Wound Healing 3
1.2.2. Chronic Wound Healing 4
1.3. Insulin as a growth factor for wound healing 6
1.4. Carriers for insulin delivery in wound healing 7
1.4.1. Lipid-Based Nanoparticles 8
1.4.1.1. Liposomes 8
1.4.1.2. Solid Lipid Nanoparticles and Nanostructured Lipid Carriers 8
1.4.2. Polymeric nanoparticles 9
1.4.2.1. Natural Polymers 9
1.4.2.2. Synthetic Polymers 10
1.4.3. Inorganic nanoparticles 11
1.5. Hydrogels for wound healing applications 11
1.6. Mesenchymal Stem Cells as tools for wound healing 12
1.7. Microfluidics for cell encapsulation 13
1.7.1. Co-encapsulation of MSc and insulin for wound healing applications 14
2. Objectives 15
3. Development of a hydrogel-nanoparticle system for topical insulin delivery 16
3.1. Materials and Methods 16
3.1.1. Materials 16
3.1.2. Nanoparticle-hydrogel production 16
3.2 Rheological Properties 17
3.3. Results and Discussion 17
3.3.1. Hydrogel optimization 17
3.3.2. Hydrogel Characterization 18
3.3.3. Experimental design 19
3.3.3.1. Viscosity 19
3.3.3.2. Spreadability 22

3.3.3.3. Mean particle size 24
3.3.3.4. Zeta Potential 25
3.3.4. Ideal formulation 27
4. Microfluidics for production of insulin-loaded alginate microparticles 28
4.1. Materials and Methods 28
4.1.1. Materials 28
4.1.2. Preparation of insulin-loaded alginate microparticles 28
4.1.3. Microparticle characterization 30
4.1.3.1. Scanning electron microscopy 30
4.1.3.2. Insulin in vitro release study 30
4.1.4. Insulin structural characterization 30
4.1.4.1. Insulin extraction 30
4.1.4.2. Circular dichroism analysis 31
4.1.4.3. Fluorescence spectroscopy analysis 31
4.1.4.4. Thioflavin T assay 31
4.1.4.5. Fourier Transform Infrared Spectroscopy 31
4.2. Results and Discussion 32
4.2.1. Microparticle Characterization 32
4.2.1.1. Scanning Electronic Microscopy 32
4.2.1.2. In vitro Insulin Release 33
4.2.2. Protein Structure 33
4.2.2.1. Circular Dichroism 34
4.2.2.2. Fluorescence Spectroscopy 35
4.2.2.3. Thioflavin T assay 36
4.2.2.4. Fourier-Transform Infrared Spectroscopy 36
5.Conclusion and future perspectives 38
References 39

List of Figures

Figure 1.1. Structure of the skin. 2
Figure 1.2. Stages of wound healing. 4
Figure 1.3. Types of nanoparticles for topical insulin delivery. 8
Figure 3.1. Viscosity (left) and spreadability (right) of the different hydrogel formulations. 18
Figure 3.2. Mean particles size (top) and zeta potential (bottom) of the different hydrogel formulations. 19
Figure 3.3. Pareto chart (left) and analysis table of ANOVA variation for the viscosity of the hydrogel. 20
Figure 3.4. Observed and Predict values graphic for viscosity as dependent variable, R^2=0.7998. 20
Figure 3.5. Structure of sodium alginate. 21
Figure 3.6. Fitted surface graphic for viscosity and sodium alginate concentration with freeze-thawing cycles (left) and glycerine (right). 21
Figure 3.7. Poly(vinyl) alcohol (PVA) structure. 22
Figure 3.8. Glycerine structure. 22
Figure 3.9. Pareto chart (left) and analysis table of ANOVA variation for the spreadability of the hydrogel. 23
Figure 3.10. Observed and Predict values graphic for spreadability as dependent variable, R^2=0.757. 23
Figure 3.11. Fitted surface graphic for spreadability and sodium alginate concentration with chitosan (left) and freeze-thawing cycles (right). 24
Figure 3.12. Pareto chart (left) and analysis table of ANOVA variation for the mean particle size of the hydrogel. 24
Figure 3.13. Observed and Predict values graphic for mean particle size as dependent variable, R^2=0.09. 25
Figure 3.14. Pareto chart (left) and analysis table of ANOVA variation for the zeta potential. 25
Figure 3.15. Observed and Predict values graphic for zeta potential as dependent variable, R^2=0.646. 26
Figure 3.16. Chitosan structure. 26
Figure 3.17. Fitted surface graphic for zeta potential dependent variable and sodium alginate concentration with chitosan. 27
Figure 4.1. Schematic of microfluidics device with “T-junction” where the continuous and dispersed phase fluids meet perpendicularly. Q denote the volumetric flow rate, and w represents the channel diameter. The subscripts “c”, “d” and “o” stand for the continuous phase, dispersed phase, and outlet channel, respectively. 29
Figure 4.2. Phase diagram in (Cac, Cad) plane for various modes observed in microcapillary flow-focusing devices. 29
Figure 4.3. Sodium tetraborate (TBS) structure. 30
Figure 4.4. Microparticles-hydrogel SEM images. Insulin-loaded alginate microparticles with cryoprotectant, alginate microparticles with cryoprotectant, insulin-loaded alginate microparticles, alginate microparticles, hydrogel with and without microparticles (from top to bottom). Scale bar: 20 µm for pictures of the first column, 80 µm for the first picture of the second column, 30 µm for the second picture of the second column, and 50 µm for the third picture of the second column. 32
Figure 4.5. Insulin release profile from insulin-loaded microparticles. 33
Figure 4.6. Photos of the different microparticles upon lyophilization. From left to right: insulin microparticles, insulin-trehalose microparticles, alginate microparticles, alginate-trehalose microparticles. 34

Figure 4.7. Far-UV CD spectra of insulin extracted from insulin-loaded alginate microparticles lyophilized with and without cryoprotectant. Insulin 0.2 mg/mL in 0.01 HCL used as reference..... 35
Figure 4.8. Fluorescence spectra of insulin extracted from insulin-loaded alginate microparticles lyophilized with and without microparticles. Insulin 0.2mg/mL in 0.01 HCL used as reference..... 36
Figure 4.9. Normalised FTIR spectra of alginate microparticles, with and without insulin, lyophilized with and without cryoprotectant..... 37

List of Tables

Table 1.1. Types of chronic wounds and its mains features. 5
Table 3.1. Matrix with the composition of the different formulations given by experimental design, based on the concentration of alginate, glycerine, chitosan, and freeze-thawing cycles..... 17

List of abbreviations and acronyms

AE Association efficiency

bFGF Basic fibroblast growth factor

CD circular dichroism

DFU Diabetic foot ulcer

ECM Extracelular matrix

FDA Food and Drug Administration

FTIR Fourier-transform infrared spectroscopy

GF Growth factors

HLA Human leucocyte antigen

hMSC Human mesenchymal stem cells

IGF-1 Insulin-like growth factor 1

MSC Mesenchymal stem cell

MMP Matrix metalloproteinase

PBS Phosphate-buffered saline

PDGF Platelet-derived growth factor

PDMS Poly(dimethylsiloxane)

PCL Polycaprolactone

PGA Polyglycolic acid

PVA Poly(vinyl alcohol)

SEM Scanning electron microscopy

TBS Sodium tetraborate

TNF-α Tumor necrosis factor-alpha

VEGF Vascular endothelial growth factor

1. Introduction

The prevalence of chronic wounds (CW) is a major public health and economic problem. Approximately 8 million people are affected by wounds worldwide, both with and without infections [1]. It has been estimated that in the USA, 2% of the entire population is affected by chronic wounds [2]. Regarding to European countries, similar data have been also reported [3], leading to a cost between 6.000€ and 10.000€ per patient every year [4]. The incidence of chronic wounds increases with age and its higher in diabetic and obese patients [5]. The treatment of acute and superficial wound is usually highly efficacious. However, treating chronic wounds is much more challenging, leading to long-term recovery due to inflammation stages [6].

The approach for chronic wound healing has been in reducing the inflammation and topical application of exogenous growth factors (GF). However, the lack efficacy of ongoing therapies have driven the research for innovative treatments and improvement of the existing ones [6]. Insulin is a low-cost growth factor known to modulate the release of inflammatory cytokines, accelerating wound healing [7]. Since it is a compatible wound dressing, the peptide hormone has been included into dressing matrices for wound treatment [8].

In this chapter, a literature review concerning the anatomophysiology of the skin, the characterization of acute and chronic wounds, and its healing mechanisms is presented. Furthermore, a theoretical explanation on the existing treatments is also presented, as well as the importance and advantages of carriers for insulin delivery in wound healing.

1.1. Anatomophysiology of the skin

Human skin is the largest organ of the body, accounting for about 15% of the total body weight in adults, that provides complex functions [9]. It protects the body against mechanical, chemical, and physical impact, as well as dehydration. Moreover, it modulates the body temperature and serves as a sensory organ. The compact part of the skin, the cutis, consists of the epidermis, a keratinized stratified *squamous epithelium,* and the underlying dermis, which is formed by connective tissue. Below the cutis is the loosely layered subcutis, which is enriched by adipose tissue. The skin layers are shown in detail in Figure 1.1 [4].

The epidermis, which is the outermost layer, is mainly composed of stratified squamous epithelium. It is further divided into four to five layers, depending on its location: *stratum corneum, stratum lucidum, stratum granulosum, stratum spinosum and stratum basal*, from the outer to the innermost layer. The primary cell type within the epidermis is the keratinocyte, and the epidermal layers represent the maturation of keratinocytes, in a process called keratinization, which allows for the development of keratin, a protein filament [10]. The *stratum basale*, the deepest layer of the epidermis, is separated from the dermis by the basement membrane [11].

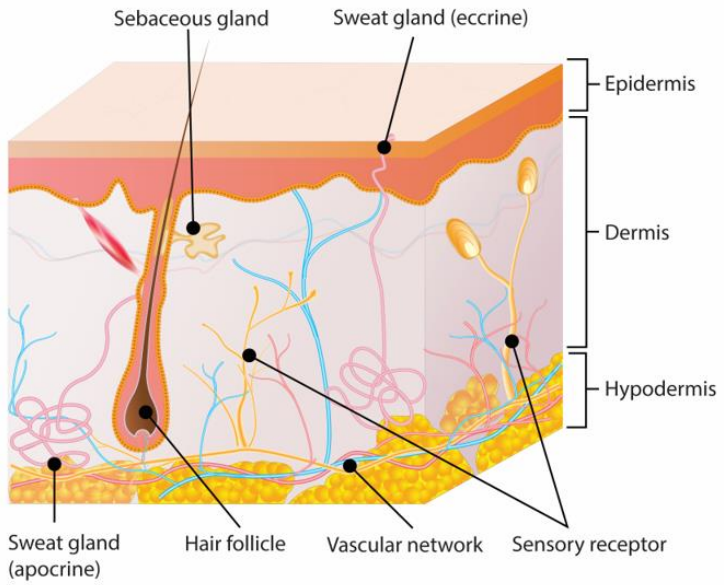

Figure 1.1. Structure of the skin. *Reprinted with permission from* [4].

The cells found in this layer, *basal cells*, are responsible for the continuous renewal of the epidermis. In the healthy epidermis, there is a balance between the processes of proliferation and desquamation, resulting in a complete renewal approximately every 28 days [12]. This layer also contains melanocytes, which produce melanin that is responsible for the pigmentation of the skin. The subsequent layer, *stratum spinosum*, also called prickle cell layer, contains a high amount of desmosomes, which are intercellular attachments formed by keratinocytes [10]. The next layer, *stratum granulosum*, contains several layers of keratinocytes with lipid-rich granules, which are responsible for the secretion of the glycolipids that keep the cells adhered to each other [13]. Above the *stratum spinosum* is the *stratum lucidum*, only present in the thick skin of soles and palms. The uppermost layer, *stratum corneum*, is formed by fully keratinized corneocytes, being a selective barrier for drug transport into the body [11, 14]. Cells within the granular layer lose their organelles and become more compact [10]. The keratinization and lipid content allows the regulation of water loss by preventing internal fluid evaporation in this layer [15].

The basement membrane, which is found between the epidermis and dermis, is a complex assembly of type IV collagen, laminin, and proteoglycans responsible for the connection of these two layers [16].The dermis is the load-handling portion of the human skin, and it is formed from collagen and elastin, providing strength and flexibility to the skin [14]. It has two layers: the papillary layer, which is the superficial one, and the reticular layer [17]. The papillary layer, with a loose connective tissue and high cell density is thin and located immediately under the epidermis [14]. On the other hand, the extracellular matrix (ECM) of the reticular dermis has a more pronounced structure, since the collagen bundles are organized into dense fibres that create an ordered network, together with elastin strands [18]. The dermis accommodates the hair follicles, sweat glands, sebaceous glands, blood vessels, nerves and sensory receptors of the skin [19, 20].

The hypodermis mainly consists of loose connective tissue, which is rich in proteoglycan and glycosaminoglycans has the function of hydrate the tissue due to the high water-binding capacity of hyaluronic acid [21]. This adipose-rich layer provides conservation of internal body heat, and is also and energy and fluid reserve that protects deeper tissues and organs [14].

Being the critical structure that shields internal tissues from mechanical damage, microbial infection, ultraviolet radiation and extreme temperature, skin is highly susceptible to injury with

significant impact to both individual patients and the healthcare economy [22]. Wounds created within the skin are result of the impact of various damaging and irritating factors leading to disruption of its continuity, while the process of their treatment is multistage and can be long-lasting [23].

1.2. Wound Healing

Severe skin injury is the result of wounds caused by incision, excision, abrasion, burn, radiation or pressure. Wound healing is a well-ordered and multi-stage process in which different cells interact with the ECM to promote skin regeneration.

The time required for wound healing depends on multiple factors, including wound size, depth, location, patient age, and local and systemic disease [24]. The degree of wounding describes the depth of damage to the respective skin layers. In first-degree wounds, only the epidermis is affected, in second degree wounds, the epidermis and dermis are affected, and in third degree wounds, all three skin layers, including the subcutis are affected. The wound healing process is highly efficient in healthy individuals. However, any deviation in this fragile response can affect the healing outcome. Parameters such as aging, comorbidities (e.g., diabetes, obesity, arterial or venous insufficiencies, autoimmune diseases), and severe burn injuries are some of the causes responsible for the delay in healing process, often due to insufficient blood supply based on impaired wound revascularization [25].

Acute wounds progress through the phases of healing in a normal and timely manner, while chronic wounds fail to progress through a normal orderly sequence of repair, without restoring normal anatomy and function [24].

1.2.1. Normal Wound Healing

The normal healing process for acute wounds follows a sequence composed of four stages: hemostasis, inflammation, proliferation and remodelling or maturation [26]. A schematic representation of these different stages is shown in Figure 1.2. Upon injury, cytokines are released, and hemostasis begins to rapidly recover the barrier function. Neutrophils, the first cells to appear at the injury site, cleanse debris and bacteria to provide a good environment for wound healing [27]. Arteriolar constriction causes a decrease in blood flow, leading to a reflex vasodilation and relaxation of the arterial vessels.

After completing hemostasis and preventing blood hemorrhage, the inflammation process occurs. The inflammatory phase starts shortly after the achievement of hemostasis, and the primary goal is to clear pathogens as well as foreign material (e.g., cytokines, platelet-derived mediators) from the wound, and to contain the damage to a localized area [28, 29]. The inflammatory response contributes to the onset of prostaglandin synthesis, which results in local vasodilation. Mast cells release histamine to increase vasodilation and vascular permeability, facilitating the movement of inflammatory cells and proteins into the extracellular space around the wound [30]. Other inflammatory mediators such as kinin and serotonin are released, boosting microvascular permeability. The hemostasis and inflammatory phase often takes 72 h to finish [27].

After about 3 days from the initial wound, the proliferative phase starts with proliferation of fibroblasts and collagen deposition. The main goal is the development of granulation tissue, which aids at restoring the vascular network while covering the damaged wound surface [31]. The angiogenesis process begins, followed by the proliferation of epithelial cells and the formation of new connective tissue and blood vessels in the wound bed. Angiogenesis is the physiological process

that allows the formation of new blood vessels to replace the damaged capillaries, providing adequate oxygen and nutrients to the wound area. Macrophages and platelets secrete the platelet-derived growth factor (PDGF), which induces fibroblast proliferation and chemotaxis. Fibroblasts migrate to the wound and move through the ECM, linking fibrin, vitronectin and fibronectin, via arginine-glycine-aspartic acid amino acid sequence. Besides, fibroblasts produce matrix metalloproteinases (MMPs), which remove impaired matrix components and enable fibroblast movement. Tumor Necrosis Factor-alpha (TNF-α) and basic Fibroblast Growth Factor (bFGF) activate endothelial cells to initiate angiogenesis. The vascularization process is also stimulated by low oxygen levels, low pH and high lactate levels [32].

Finally, on the remodelling phase, novel epithelium is developed along with scar formation. In acute wounds, the levels of collagen increase, promoting wound tensile strength [33]. Glycosaminoglycans and proteoglycans, components of the ECM, provide strength, support, and density [34]. Regular collagen formation and disintegration, as well as remodelling of the ECM are completed within 3 weeks of trauma until a steady shape is reached. Due to the interactions between the ECM and the fibroblasts, the wound edges approach, and the connective tissue size diminish.

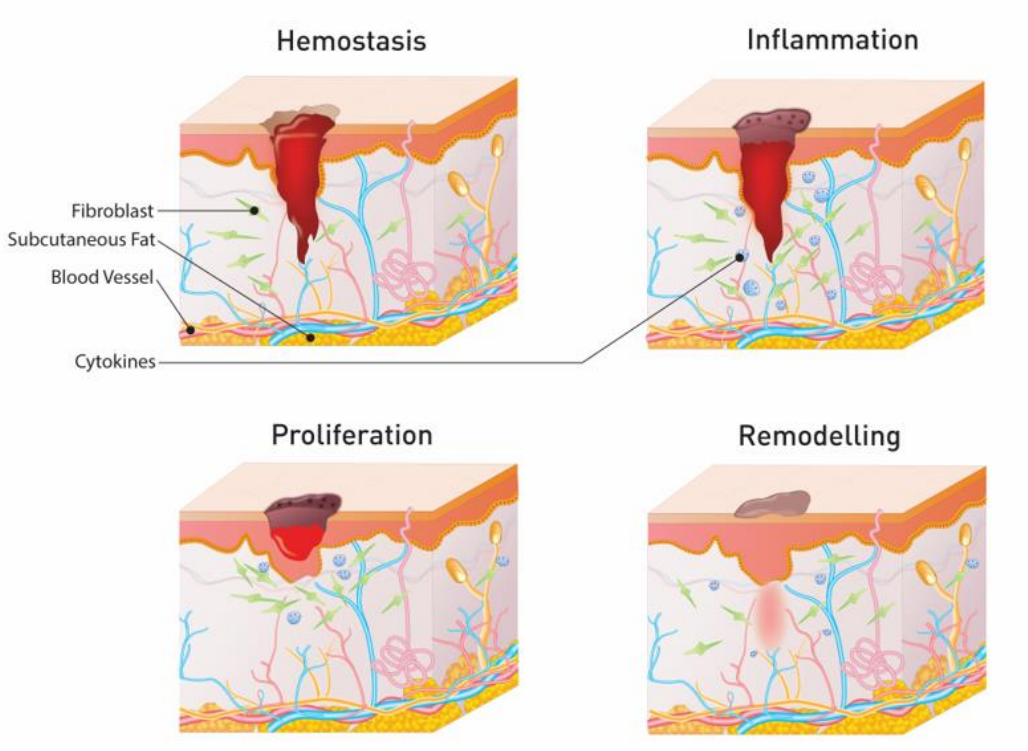

Figure 1.2. Stages of wound healing. *Reprinted with permission from* [4].

1.2.2. Chronic Wound Healing

A chronic wound occurs when the repair process is disrupted, and the healing is subsequently delayed. Chronic wounds, namely pressure ulcers, diabetic ulcers, and venous ulcers, have a prolonged inflammation and do no heal within 12 weeks (Table 1.1) [35].

Table 1.1. Types of chronic wounds and its mains features. *Adapted with permission from* [4].

Wound type	Etiology	Microenvironment	Bacterial environment	Average healing time	Ref.
Pressure Ulcers	Spinal cord injury Paralysis Senility Substance abuse Malnutrition Stroke Multiple sclerosis	Shear stress Friction High Humidity Temperature Tissue atrophy	*Enterococcus* *Staphylococcus* *Pseudomonas* *Serratia* *Proteus* *Corynebacterium* *Staphylococcus* *Anaerococcus* *Bacteroides*	2 weeks	[42-44]
Diabetic foot ulcers	Hyperglycemia Poor circulation Neuropathy Wounded feet	Ischaemia Infection Foot deformity Callus Trauma Pressure	*Enterococcus* *Pseudomonas* *Streptococcus* *Serratia* *Staphylococcus* *Anaerococcus* *Corynebacterium* *Pseudomonas*	6 months	[45-47]
Venous leg ulcers	Age Obesity Physical inactivity Trauma Deep vein Thrombosis Phlebitis	Chronic venous hypertension Vein walls structural failure Valve system failure	*Staphylococcus* *Serratia* *Streptococcus* *Pseudomonas* *Corynebacterium* *Staphylococcus* *Bacteroides*	4 months	[48, 49]

These wounds have high levels of MMPs, an increase of inflammatory cytokines release, debris and infection [36]. As the microbial load on the wound expands, healing is considerably interrupted. During the inflammatory response occurs the release of an excessive amount of reactive oxygen species (ROS) and inflammatory cytokines, leading to a continuous stage of inflammation and proteolytic enzymes. Increased levels of protease in the wound result in the deterioration of local proteins (e.g., ECM proteins and GFs), matrix component reduction, epithelialization process disturbance and wound contraction failure [37, 38]. Furthermore, macrophages and other important elements such as fibroblasts and stem or tissue progenitor cells become unable to migrate and help in the closure process [29]. Finally, fibroblasts no longer respond to inflammatory mediators and GFs, resulting in a decreased proliferative capacity [39, 40].

All of these molecular and cellular changes prevent the deposition of ECM and the formation of granulation tissue, leading to the formation of chronic wounds [29]. Thus, chronic wounds are characterized by excessive inflammation, hypoxia, high biological bioburden, prolonged protease activity, neuropathy and, in case of irreparable tissue damage, fibrosis. Once chronic inflammation is stagnant or devitalized tissue is surgically removed, so the ideal therapy for chronic wounds is to prevent infection and promote healing in the same way as the acute wounds [41].

1.3. Insulin as a growth factor for wound healing

GFs are biomolecules that effectively regulate the specific functions and growth activity of cells constituting tissues [50]. The application of GFs such as epidermal growth factor (EGF) and transforming growth factor beta (TGF-β) in wound healing treatments has been tested ad a method of promoting faster recovering by stimulating skin cells to migrate and proliferate more rapidly [51].

Insulin, a peptide hormone and GF mostly known to regulate blood glucose levels, plays an important role in the dynamic process of wound healing. In contrast with other GFs, insulin is low-cost, available in a highly pure crystalline form, and is compatible with biomaterials commonly used in wound dressings and drug delivery systems [52]. Insulin is one of the most highly conserved peptides found in vertebrates and generally differs by 1-3 amino acids between species [53]. Insulin is industrially produced using recombinant DNA technologies, which alleviates the need for animal sourced organs, and is a cost-effective approach in large scale production [54, 55]. The crystallization process of purified insulin is also necessary to ensure the stabilization of the peptide [52].

It has been described that insulin increases protein synthesis in skin and stimulates growth and development of different cell types, affecting proliferation, migration, and secretion of keratinocytes, endothelial cells, and fibroblasts [56-60]. Kabalak et al. (2013) studied 23 cases of severe burn patients with normal glucose levels. Half of these patients received insulin treatment and it was observed a decrement of pro-inflammatory proteins and serum triglyceride levels. It was also observed that the same treatment decreased patient morbidity and mortality when compared to the non-insulin patients [61].

In 2012, Chen and Zhang studied the inflammatory response after topical application of insulin in mice submitted to full-thickness excision wound. The authors concluded that wound closure was reduced from 7 to 5 days in animals treated with insulin, which was a result of supressed neutrophil infiltration [62].

Azevedo et al. (2016) studied the effects of topical insulin application on wound healing in rats subjected to second-degree burns on the increase of collagen retention, stimulation of the microvascular network, and depression of the inflammatory phase [63]. The animals were divided into 4 groups: diabetic rats receiving topical insulin cream, diabetic rats receiving placebo, healthy rats receiving topical insulin cream, and healthy rats receiving placebo. Histological examination showed increased Type II collagen levels between days 1 and 7 in healthy and diabetic wounds treated with insulin cream, compared to diabetic wounds treated with placebo. Angiogenesis and inflammatory response were significantly higher at 2 weeks postburn in wounds treated with insulin cream to levels related to those of healthy rats receiving topical insulin cream and placebo [63].

In 2017, Zhang and colleagues studied the efficacy of local insulin application regarding WH rate, dropping of blood sugar, and potassium levels, since these signs appear in intravenous insulin administration. Therefore, an insulin-zinc solution was injected locally in the wound and every other day into white male New Zealand rabbits. It was noticed a higher healing rate among rats with localized insulin therapy when compared to intravenous treatments cohorts [64].

Concerning the vulnerable structure of insulin, Li and co-workers developed an effective topical insulin delivery system by encapsulating the GF into microparticles, which were later incorporated in a silk fibroin sponge [65]. The molecular structure of insulin was maintained, and the authors observed an extended release for 30 days. Furthermore, the in-vivo restorative effect of the matrix wound dressing was assessed in full-thickness diabetic wounds of Sprague-Dawley rats. After 3 weeks, the histological analyses revealed strong cell relocation, collagen deposition, and epidermis, when compared to the control group [65].

1.4. Carriers for insulin delivery in wound healing

Among the several products considered for topical administration, silver nanoparticles are often used in creams, gels, or dressings due to their effectiveness in hospital-acquired infections caused by antibiotic resistant bacteria, and local therapy of infected wounds [66]. Silver nanoparticles are commonly used in wounds dressings and other several products, because silver has anti-inflammatory and antimicrobial properties, as well as collagen control regulation, inducting its proper arrangement during wound closure [67].

In the past few years, several commercially available products have emerged with the use of GFs for wound healing. Regranex gel (Healthpoint Biotherapeutics, Fort Worth, TX, USA) contains recombinant human PDGF. Regranex has been approved by FDA for the prevention of lower-limb amputations in the cases of diabetic foot ulcers (DFUs) [68]. Patients with diabetic wounds treated with topical PDGF experienced around 40% wound closure increase, compared to control group [69].

Johnson & Johnson has developed Program for topical wound therapy in the form of sterile, lyophilized, oxidized regenerated cellulose and collagen, deactivating the wound bed proteases, and protecting the GFs that are present in the wounds. Recently, homologous platelet-rich plasma (PRP) was used for the treatment of chronic wounds, as thrombin activates platelets releasing mitogenic and chemotactic factors throughout the wound healing process. For this reason, Nuo Therapeutics, Inc, (Gaithersburg, MD, USA) developed the AutoloGel™ indicated for the treatment of non-healing chronic wounds [70]. AutoloGel is a platelet-rich plasma gel that should be topically administered twice a week. PRP is defined as a portion of the plasma fraction of autologous blood with a platelet concentration above baseline [71]. Besides, it has both mitogenic and chemotactic properties and acts as a growth factor agonist [72].

Insulin has been showed promising results for cutaneous wound care, but its low stability in the wound bed is an important drawback. Therefore, its encapsulation into carriers has been suggested as a promising strategy [73]. There are different types of nanoparticles (Figure 3) under consideration for topical delivery of insulin, which are mostly from lipid, polymer, or inorganic origin.

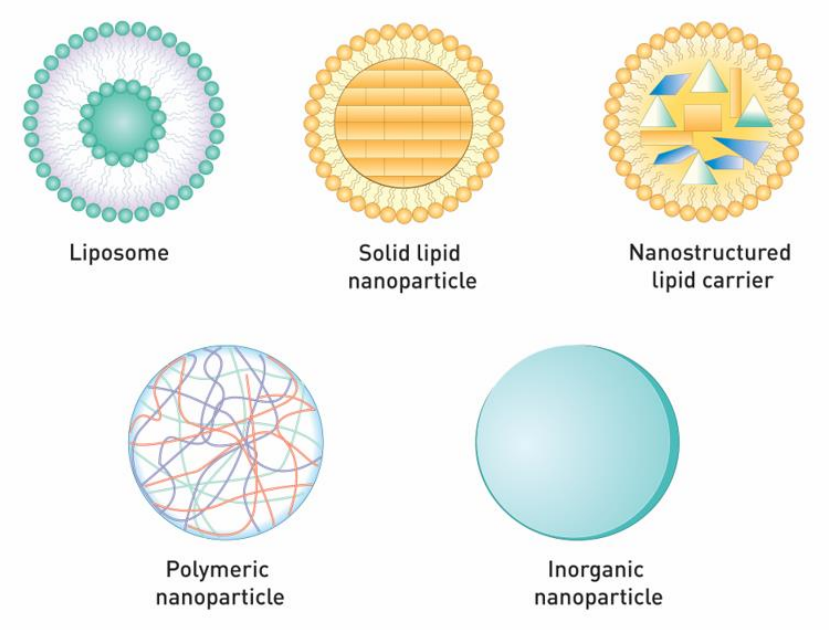

Figure 1.3. Types of nanoparticles for topical insulin delivery. *Reprinted with permission from* [4].

1.4.1. Lipid-Based Nanoparticles

Lipid-based nanoparticles, such as liposomes, solid lipid nanoparticles (SLN) and nanostructured lipid carriers (NLC) are commonly used for topical application because they allow a sustained drug release, with adequate skin absorption [74].

1.4.1.1. Liposomes

Liposomes are formed by at least two lipophilic layers, with a dimension between 100 and 1000 nm [75]. They can load hydrophobic and hydrophilic drugs and are typically composed of phospholipids consisting of a polar head and two nonpolar chains. Liposomes have been widely used for topical drug administration because of the presence of lipid bilayers that mimic the cell membrane of the human body [76]. Furthermore, wound dressings made of gauzes impregnated with liposomes have been used in infected wounds showing drug release and more accurate management of chronic topical inflammation [77]. However, liposomes have revealed poor long-term stability leading to reduced encapsulation efficiency, low reproducibility and uncontrolled drug release during storage [78].

1.4.1.2. Solid Lipid Nanoparticles and Nanostructured Lipid Carriers

Solid lipid nanoparticles (SLN) are small carriers of solid lipids at body and room temperature, which were developed to overcome liposome limitations [79]. They have increased drug permeation

through skin and are biocompatible, biodegradable, and easily prepared on large scale [80]. For those reasons, SLN have been used has delivery platforms for topical administration.

Nanostructured lipid carriers (NLC) are second generation lipid nanoparticles generated to improve drug loading, being composed of a mixture of solid and liquid lipids [4]. Therefore, they provide prolonged drug release, as well as reduce drug expulsion during storage [81]. There are no relevant studies concerning the delivery of insulin using SLN and NLC, but both lipid nanocarriers have been used on injured skin showing their ability to topically deliver GFs in a sustained and controlled manner [4].

Gainza and co-workers used SLN and NLC to deliver the recombinant human epidermal growth factor (rhEGF) to wounds, obtaining a co-encapsulation efficiency of 74% and 96% for SLN-rhEGF and NLC-rhEGF, respectively. The topical administration of 10 and 20 µg of both SLN-rhEGF and NLC-rhEGF in a full thickness excisional wound in diabetic mice exhibited decreased wound area in comparison to empty lipid nanoparticles and untreated control [82]. The results were not significantly different between the 10 and 20 µg doses [82]. The same authors, in another study, evaluated the efficacy of rhEGF-loaded NLC in a full-thickness excision wound model in pigs. The topical application of 20 µg of rhEGF-NLC twice weekly promoted a faster rate of healing, when compared with the group treated with 75 µg of free rhEGF and unloaded NLC. It was also demonstrated that the application of rhEGF-loaded NLC stimulates angiogenesis stimulated angiogenesis, cell migration and proliferation, as well as collagen deposition [83].

1.4.2. Polymeric nanoparticles

Polymers are macromolecules composed of repeated monomer units, where their chain length depends on the number of the monomer units as well the molecular weight of these individual monomers. The knowledge of polymer-based compounds has been increasing, which allowed some structural modifications. The polymeric materials may come from natural and synthetic origin, being used separately or mixed together for many applications, including wound healing [84].

1.4.2.1. Natural Polymers

Chitosan, hyaluronic acid, cellulose, alginate, and collagen are polymers with natural origin, which have been widely used to obtain nanocarriers. Chitosan is a chitin-derived polymer composed of D-glucosamine and N-acetyl-D-glucosamine. Chitin can be found in the crustacean shells, insect bone, and fungal mycelia [85]. Chitosan is a polysaccharide widely used in topically applied vehicles due to its biocompatibility, biodegradability, low toxicity, and angiogenesis promoter [86]. Moreover, chitosan-based materials show positive charge, which offers mucoadhesiveness, haemorrhage control, and wound healing stimulation [87]. Ehterami and co-workers used ionotropic gelation to formulate chitosan nanoparticles loaded with insulin, which were incorporated into an electrospun poly(ε-caprolactone)/collagen. These wound dressings were applied onto 1.5 x 1.5 cm^2 full-thickness wounds on the back of Wistar rats. After 2 weeks of treatment, wounds revealed epidermal and granulation tissue formation with a scab, while the rats of control group showed approximately 60% of wound length [88]. Despite the benefits described previously, chitosan-based formulation are not yet acceptable for scale-up production because of its limited production reproducibility [89].

Alginate is a polysaccharide obtained from brown algae, consisting of different amounts of (1-4)-linked β-D-mannuronic acid (M) and α-L-guluronic acid (G). These G residues favour gelation in the presence of divalent ions, enabling the formation of particles. Alginates and its salts present

haemostatic and regenerative characteristics that have been used for wound dressings, stimulating cell migration, enhancing angiogenesis, and decreasing proinflammatory cytokine levels in chronic wounds. Due to their hydrophilic nature, alginate dressings maintain a moist environment, absorbing wound exudate and restricting bacterial infections at the wound site [90]. In 2010, Borselli et al. formulated an injectable alginate gel containing both insulin-like growth factor-1 (IGF-1) and VEGF and delivered it in ischemic mice. Only IGF-1 treatment reduced the apoptosis process and increased cell activation and proliferation, leading to the considerable reconstruction of muscle fibers at the wound site. IGF-1 showed an *in vitro* release of approximately 80% in the first 24h, in contrast to VEGF, which presented a sustained release profile showing an *in vitro* release of approximately 40% in the first 24h [91].

Hyaluronic acid is involved in all phases of the healing process, contributing to the reduction of ROS at the wound site [92]. It is regularly used in wound healing to promote tissue repair due to its moisturizing ability, proliferation promotion, and capacity to induce inflammatory signals [93]. In 2010, Hirakura et al. developed a hyaluronic acid-based hydrogel involving nanogels from cholesteryl group with insulin to perform *in vitro* and *in vivo* release studies. The authors observed a sustained and controlled release of insulin due to the crosslinking degree without bioactivity loss [94].

Although natural polymers offer biocompatibility and biodegradability, only with synthetic polymers is possible to control the structure, providing tailorable properties.

1.4.2.2. Synthetic Polymers

Synthetic polymers, such as polycaprolactone (PCL), polylactic acid (PLA) or polyvinyl alcohol (PVA) have been extensively used in regenerative medicine [95]. PLGA is a copolymer formed by glycolic and lactic acid with biodegradability and sustained release control properties, commonly used to produce nanoparticles [96-98]. The release of lactase, during its degradation, promotes the formation of new blood vessels [98]. Hrynyk et al. (2012) developed PLGA carriers containing insulin, which were incorporated into an alginate-containing PEG sponge. This wound dressing formed a hydrogel, providing protection and a moist environment essential for wound healing. A sustained release profiled was maintained up to 21 days, with demonstration of migration rates if human epidermal keratinocytes for 10 days, when compared to 10^{-7} M insulin solution [99]. In 2018, Abdelkader et al. studied the delivery of inulin-loaded PLGA nanoparticles embedded in a PVA-borate hydrogel. The authors observed faster cell proliferation in human fibroblasts (Hs27) and keratinocytes (HaCaT) in cell scratch assay following the addition of nanoencapsulated insulin, when compared to free insulin conditions [100]. In another approach, PLGA nanoparticles loaded with insulin were developed by a modified double emulsion solvent evaporation technique and incorporated in a PVA-borate hydrogel [73]. The hydrogel was used to evaluate wound healing in healthy and diabetic rats. Healthy and diabetic mice treated with the developed hydrogel incorporating the insulin-loaded PLGA nanoparticles exhibited faster wound healing, when compared with diabetic and healthy mice receiving free insulin incorporated into the hydrogel [73].

PVA is known to be a truly biodegradable synthetic polymer since the early 1930s [101]. It is a noncarcinogenic, non-toxic, biocompatible, water-soluble, and inexpensive polymer with favourable physical properties such as good transparency, low interfacial tension, and high swelling ratio [102]. However, its biodegradability depends on the parameters, such as the degree of polymerization, degree of hydrolysis, distribution of hydroxyl groups, or crystallinity [103]. Therefore, the degradation rate of PVA could be controlled by modifying these parameters [103]. PVA is usually prepared into hydrogels with excellent viscoelasticity, that have already been used in wound healing

[104]. Despite these properties, the commonly prepared PVA hydrogels have poor mechanical properties, which severely limits their potential applications [105, 106]. In order to enhance the mechanical strength of PVA, many researchers have carried out investigations. The creation of crystalline regions in PVA through physical crosslinking improves its mechanical integrity and reduces the respective water absorption capacity [107], which reduces the PVA degradation rate once in contact with body tissues [108].

1.4.3. Inorganic nanoparticles

Inorganic nanoparticles have a minor impact concerning topical insulin delivery. However, there are different inorganic nanoparticles with potential for regenerative medicine. Metal nanoparticles, such as silver nanoparticles (AgNPs), are submicron particles of metallic or magnetic origin [109]. Silver nanoparticles show antibacterial activity against a wide range of bacteria without developing microbial resistance and are easily obtained by inexpensive methods [110]. Therefore, this type of nanoparticle can be used in wound dressings. In 2010, Liu et al. studied the effect of silver nanoparticles and silver sulfadiazine on dermal contraction, and epidermal re-epithelization in a full-thickness excisional wound model on mice. Wounds treated with AgNPs showed faster closure, higher rate of fibroblast differentiation, and increased proliferation of keratinocytes, when compared to silver sulfadiazine-treated wounds [111].

Silica or silicon dioxide nanoparticles are also effective for wound healing applications because they have versatile properties such as low toxicity, molecular stability, targeted delivery, and easy production [112]. Quignard et al. studied the influence of silica nanoparticles on the wound healing process, by applying 50 and 100 μM of nanoparticles in an *in vitro* wound healing assay using human dermal fibroblasts (CCD-25SK). The authors observed that both concentrations stimulated cell viability and proliferation versus the control group, after 3 days of treatment [113].

1.5. Hydrogels for wound healing applications

To optimize wound healing, the wound must be clean, with a healthy granulating base, and free of infection. Debridement, or removal of nonviable wound tissue, is essential to prepare the wound bed for healing, allowing the migration of keratinocytes. Addressing local infection using cleansing agents and topical antimicrobials is also essential to improve healing. Topical agents can reduce superficial wound infection, but systemic antibiotics should be used in cases of deep or systemic infection. It is also important to ensure an adequate moisture balance because it promotes keratinocyte migration and improves wound healing. Wound dressings are manufactured using natural or synthetic polymer in various forms such as hydrofibers, hydrocolloids, foams and hydrogels [114]. Alginates are ideal for very exudative wounds because of their high fluid absorbance. Hydrogels are mostly used to maintain a most environment and ensure fluid exchange, being suitable for dry wounds. Foams and hydrocolloids are only used in minimally exuding wounds because of their limited fluid volume. Overall, these options tend to have one singular function: antibacterial activity, absorption or pH regulation. The combination of these multiple treatments is often the option required to provide effective patient care and to stimulate chronic wound healing [114].

Safe and rapid wound healing requires precise maintenance of an optimal moisture level and proper gas circulation, as well as the dressing ability to absorb excess exudate [115]. Due to their similarity

to living tissues in terms of water content, soft and rubbery consistency and low interfacial tension with water or any biological fluids, hydrogels seem to be the most promising dressing for wound healing [116-118]. The porous structure of hydrogels can help absorb wound exudate, reduce the chance of infection, and create and environment to accelerate the wound healing process [119]. Hydrogels are crosslinked networks of hydrophilic polymers, which can be natural or synthetic, which can be chemically, physically, or ionically crosslinked, leading to a dramatic increase in viscoelastic properties and the maintenance of shapes and volumes in aqueous environments [120]. They can also be further tailored to incorporate various cell-interactive moieties to facilitate stem cell-based therapy by promoting cell viability and directing stem cell differentiation to target tissues. Recently, Yuan et al. (2021) designed a novel double cross-linked hydrogel suitable for dynamic wounds. The unique double cross-linked structure of the hydrogel resulted in better physicochemical properties, such as faster gelation time, stronger mechanical property, and enhanced adhesive strength. Moreover, the results showed acceleration in the reconstruction of skin structure and function [121].

1.6. Mesenchymal Stem Cells as tools for wound healing

Over the last quarter century, interest in human mesenchymal stem cell (hMSC) research has accelerated due to their potential in regenerative medicine, tissue engineering, and cell-based therapies [122]. Stem cell transplant has been recognized as a promising strategy to induce the regeneration of injured and diseased tissues and sustain therapeutic molecules for prolonged periods *in vivo* [120]. Mesenchymal stem cells (MSCs), a type of pluripotent stem cell, are a particularly attractive source for cell therapies because of their multiple beneficial properties, such as self-renewal capacities and ability to differentiate into different cell lineages [120, 123]. Additionally, one of the most prominent types of stem cell mediators are GFs since they are known to have a wide array of modulatory effects on the properties of MSCs [124]. These properties include their mobilisation, proliferation rate, differentiation potential, and survival [125, 126]. Therefore, the co-encapsulation of GFs with MSCs in microparticles could be a promising approach to provide long-term bioactivity in the wound bed. MSCs can be isolated from different tissues (e.g., bone marrow, adipose tissue, skeletal muscle, dental pulp) and foetal tissues (e.g., placenta, amniotic fluid, and umbilical cord), and have the potential to differentiate into at least osteoblasts, chondrocytes and adipocytes [120]. At normal conditioned culture media, MSCs manifest characteristics of plastic adherence and exhibit a morphology similar to fibroblast, having the positive expression of CD73, CD90, CD105, and lack expression of CD45, CD34, CD14, CD19 and HLA-II [127]. Studies have shown that topical application of MSCs have improved wound healing and angiogenesis, while injections of MSCs can decrease inflammation and increase vascular endothelial growth factor (VEGF) [128-130]. Additionally, recent evidence suggests that the MSC *secretome*, which is comprised of angiogenic factors, hormone, cytokines, GFs, and ECM proteases, plays an essential role in reparative processes, enhancing angiogenesis and ECM deposition [131, 132]. Thus, when it comes to wound healing, MSCs can be truly relevant, not only because of their mechanism influencing skin restoration, but also because of their ability to manipulate the microenvironment aided by GFs and cytokine release [127, 133]. Studies have reported that the MSC-conditioned media improves wound healing by reducing inflammation, improving cellular functions, and enhancing granulation tissue formation [134, 135]. However, it has been stated that the majority of exogenously applied MSCs may not survive nor were detectable incorporated in the target area, what evokes some doubts about the effectiveness of the adult stem cells [136]. To overcome this problem, it is crucial

to develop new methods of improving the survival and homing capacity of MSCs, such as the co-encapsulation with insulin, in order to increase the therapeutic efficacy in damaged skin [136].

1.7. Microfluidics for cell encapsulation

Microfluidics is particularly attractive for cell encapsulation since it provides a rapid and reproducible methodology for microgel generation of controlled size and simultaneous cell encapsulation [123]. With the outstanding biophysical and biochemical properties of microgels, droplet-based microfluidics has exhibited huge potential for various applications, such tissue engineering [137]. Microfluidics devices are miniaturized platforms with specific flow characteristics that control the formation of multiple emulsions within micron-sized channels [138].

Droplet-based microfluidics can be divided into two methods: active (e.g., centrifugal, electric, and magnetic methods) and passive (e.g., cross-flowing, flow focusing and co-flowing methods).

Passive droplet-based microfluidics use two immiscible phases in which aqueous droplets containing cells are formed in the dispersed phase by flow shearing [120]. This technique generates a large number of monodisperse droplets, typically in the range of 10-100 μm, within a short period of time [139]. The T-junction configuration, which are used to form aqueous droplets in the oil phase, allows the shear force imposed by an immiscible flow fluid to generate droplets at the intersection of two perpendicularly positioned microchannels [140-142]. The cell-laden solution is subjected to shearing off by a water-immiscible continuous fluid (e.g., oil phase), resulting in the formation of dispersed particles with well-defined shapes and sizes [120]. This technology can provide encapsulation of a single cell within a droplet, which allows for high-throughput single cell screening and analysis capabilities [143, 144]. In dripping mode, because of large viscous shear force, the dispersed phase breaks up before the growing droplet obstructs microchannels, so the droplet retains a spherical shape and a size smaller than the channel dimension [145].

Among all the parameters that can influence the size and the generation rate of droplets, the viscosity of the fluids, particularly one for the continuous phase (i.e., oil carrier), is one of the dominants since it is highly related to the capillary number (Ca) that affects the droplet break-up [146]. Ca represents the relative effect of viscous drag forces compared with surface tension forces that act on an interface between two immiscible liquids. The droplet generation rate is algo highly dependent on the flow rates of both oil and water solution [147].

Mesquita et al. (2021) developed a microfluidic system based on two different types of geometry able to encapsulate and manipulate individual spheroids in small drops. Cellular spheroids are three-dimensional models formed by a suspension of cells with self-assembly [148]. The microdroplet generation was achieved with effectiveness and robustness. Furthermore, the encapsulation of spheroid allowed the generation of tissue-like constructs than can be used for bioprinting applications [138].

In 2020, Chuanfeng et al. presented a microfluidics-based method for continuous encapsulation of MSCs in monodisperse alginate microgels to boost bone regeneration by providing a controlled osteogenic microenvironment. The developed microfluidic technique allowed the encapsulation, gelation, and de-emulsification into a one-step fabrication. MSCs encapsulated in Ca-alginate microgels showed enhanced osteogenesis and displayed significantly enhanced bone formation compared to MSCs mixed with microgels and acellular microgels in a rat tibial ablation model [149].

1.7.1. Co-encapsulation of MSCs and insulin for wound healing applications

Therapeutic use of insulin has been associated with a short-life *in vivo* due to the presence of proteases in the wound bed. Hence, the development of a suitable and effective delivery strategy is critical for improved chronic wound regeneration [150]. Insulin encapsulation ensures proteolysis preventing, maintaining the amino acid chain and the three-dimensional protein arrangement [151].

By definition, microspheres are spherical polymerized networks with a diameter of 100-400 μm [150]. Cellular environments created by microcapsules can be engineered to encourage transplanted cells to exhibit multiple biological functions, aiding tissue regeneration by direct differentiation and/or growth factor secretion [120]. Besides, they provide biomimetic three-dimensional (3D) extracellular microenvironment to generate microtissue stimulating positive cell-cell interactions and extracellular matrix (ECM) formation [152].Their small size and increased surface area offer occlusive properties and moisturizing effect, as well as intracellular entry and transfer facility throughout the skin layers [153].

The microparticles capacity to provide controlled and sustained release avoid the need of a frequent administration, which proves that they really are a valuable strategy for chronic wound treatment [151]. The encapsulating agents need to have feasible properties, such as good dissolution, and they need to easily allow to obtain carriers able to increase the adherence capacity and residence time of the system in the target sites [154-156]. Thus, the influence of loading MSCs together with insulin into the alginate microparticles may be a strategy to explore to improve the maintenance of the growth factor structure when in the wound bed.

2. Objectives

The aim of this work is to develop a hydrogel-microparticle delivery system for topical administration of insulin for wound healing applications. Therefore, it can be subdivided in two parts:

1. The first objective is to develop a hydrogel with insulin-loaded nanoparticle by freeze-thawing. PVA is the synthetic polymer used to produce this hydrogel with viscoelastic properties and able to provide comfort sensation when applied in the wound site. Freeze-thawing cycles were applied to the hydrogel formulations to enhance the mechanical properties of PVA. Alginate is also used in the composition of this hydrogel due to its ability to maintain a moist environment, absorbing wound exudate and restricting bacterial infections at the wound site. Finally, glycerine is also part of the hydrogel working as moistener and emollient. Nanoparticles coated with chitosan were produced to study the rheological properties of the hydrogel and optimize the formulation.

2. In a second phase, the objective is to develop a delivery system co-encapsulating insulin and MSCs by microfluidics. In this case, the aim is to evaluate the structure of insulin upon encapsulation to later encapsulate the MSCs.

3. Development of a hydrogel-nanoparticle system for topical insulin delivery

In this chapter is presented the materials and methods regarding the preparation and optimization of the hydrogel obtained by freeze-thawing, for insulin delivery, as well as the results obtained regarding its rheological properties and optimal formulation. To perform these studies, insulin-loaded nanoparticles coated with chitosan already prepared were also used.

3.1. Materials and Methods

3.1.1. Materials

For the hydrogel production it was used PVA from Sigma-Aldrich (St. Louis, EUA), sodium alginate (very low viscosity) from Alfa Aesar (Massachusetts, MA, United States) and pharmaceutical glycerine from Ceamed (Funchal, Portugal).

For the nanoparticles already prepared, it was used PLGA 50:50 Resomer RG 503 H (Mw 24,000-38,000; Tg 44-48◦C) from Evonik Industries AG (Essen, Germany), chitosan (low molecular weight) and recombinant human insulin from Sigma-Aldrich (St. Louis, EUA), dichloromethane from Thermo Fisher Scientific (Waltham, EUA), hydrochloric acid 1M and Acetic Acid glacial from Panreac (Barcelona, Spain).

Different solutions were prepared with different reagents, and it was used milli-Q water, produced in-house, as the solvent for all solutions.

3.1.2. Nanoparticle-hydrogel production

To evaluate and optimize the hydrogel properties, insulin-loaded nanoparticles coated with chitosan previously prepared were used. The nanoparticles were produced using a solvent emulsification-evaporation method according with a water-in-oil-in-water (w/o/w) double emulsion technique developed by our group [157]. Once produced, the nanoparticles were coated with chitosan. Different amounts of a 1.5% (w/v) chitosan in 1% acetic acid (v/v) solution were added to the nanoparticles solution and let to coat for 4 h. Unloaded nanoparticles both with and without chitosan coating were also considered. Once produced, the nanoparticles were incorporated into a polymer solution for gelification by freeze-thawing. Then, sodium alginate and glycerine were added to the nanoparticle suspension in different amounts and dissolved in magnetic stirring. After this, the formulations were subjected to freeze-thawing cycles, in periods of 6 hours to freeze, using a freezer at -20°C from Liebherr Group (Bulle, Switzerland), and another 6 hours to thaw.

The hydrogel was optimized using the Statistica software version 10 by TIBCO Software (Palo Alto, USA), according to a quality by design approach. The concentration of chitosan, sodium alginate and glycerine, as well as the number of freeze-thawing cycles were the independent variables. The effect of these parameters was assessed by evaluating the viscosity and spreadability of the hydrogel, as well as the mean particle size and zeta potential, which are the dependent variables. Therefore, it was chosen a model with 4 factors (independent variables) and 4 blank columns for the dependent variables and the software returned a matrix with the hydrogel composition for each experiment. Finally, the Design-Expert program (version 6.0.4) by Stat-Ease Inc (Minneapolis, USA) was used to obtain the optimal hydrogel formulation.

3.2 Rheological Properties

To assess the viability of the hydrogel for topical application the rheological properties of the hydrogel were analysed by evaluating its viscosity and spreadability.

The viscosity of the hydrogel was evaluated with a DV-II+Pro Viscometer from AMETEK Brookfield (Middleborough, United States) with an CPE-52 spindle. It was used a 500 µL sample of the hydrogels until 100%, approximately, was reached for torque value.

The spreadability was assessed by dropping 500 µL in a centre marked glass plate, on top of millimetric paper. Predetermined weights of hydrogel were place on top of another glass plate, with an interval of 1 minute. To calculate the mean diameter of the hydrogel spread, the diameter in opposite direction was measured for all samples. Three weights (48.6g, 251.8g and 778g) were considered, and the spreadability (Ei) for each sample was calculated according with the following equation:

$$Ei = d^2 \frac{\pi}{4} \tag{3.1}$$

Where d is the diameter calculated.

For size and zeta potential analysis, the particles hydrodynamic radius and superficial charge were analysed by dynamic light scattering and electrophoretic light scattering, using a Zetasizer Nano series from Malvern Panalytical (Malvern, United Kingdom). To perform these experiments, the samples were diluted with milli-Q water, and all measurements were run in triplicate.

3.3. Results and Discussion

3.3.1. Hydrogel optimization

Table 3.1. Matrix with the composition of the different formulations given by experimental design, based on the concentration of alginate, glycerine, chitosan, and freeze-thawing cycles.

Formulation	Alginate %(w/v)	Glycerine (%v/v)	Chitosan %(w/v)	Freeze-Thawing Cycles
A	1.0	5.0	0.25	1.0
B	1.0	5.0	0.75	3.0
C	1.0	10	0.75	1.0
D	1.0	10	0.25	3.0
E	1.5	7.5	0.50	2.0
F	1.5	7.5	0.50	2.0
G	1.5	7.5	0.50	2.0
H	2.0	5.0	0.75	1.0
I	2.0	5.0	0.25	3.0
J	2.0	10	0.25	1.0
K	2.0	10	0.75	3.0

The hydrogel composition was optimized following an approach which consist of varying the concentration of alginate, chitosan, and glycerine, as well as the number of freeze-thawing cycles. The concentration of sodium alginate varied between 1-2% with a centre point of 1.5%, and glycerine concentration between 1.5-10% with a centre point of 7.5%. Statistica software returned a matrix with 11 formulations, after received these variants. This matrix is showed in Table 3.1.

3.3.2. Hydrogel Characterization

To find an optimal hydrogel formulation, with good rheological properties for topical application, different hydrogel formulations were submitted to viscosity and spreadability tests. The results obtained for these two parameters are shown in figure 3.1. Regarding to formulation A, B, C and D, the results show very low viscosity and high spreadability. Since the ideal viscosity for topical application falls in the range of 1,000-10,000 cP, these formulations, which showed lower viscosities than 1,000 cP, are not suitable for the delivery system. In the other hand, the formulations H, I and K, presented high viscosity and low spreadability. According with expectations, it is possible to conclude that the more viscous is the formulation, the less it spreads. This relationship can be explained by the fact that with the increase in viscosity comes the necessity of a higher force to spread the hydrogel. The viscosities of the formulations E, F, G, which are between 1,000 and 2,000 cP, can be considered in the lower to medium range. Therefore, these three formulations can be considered suitable for the hydrogel-microparticle system.

The mean particle size and zeta potential were also evaluated. The results obtained for each formulation are shown in Figure 3.2.

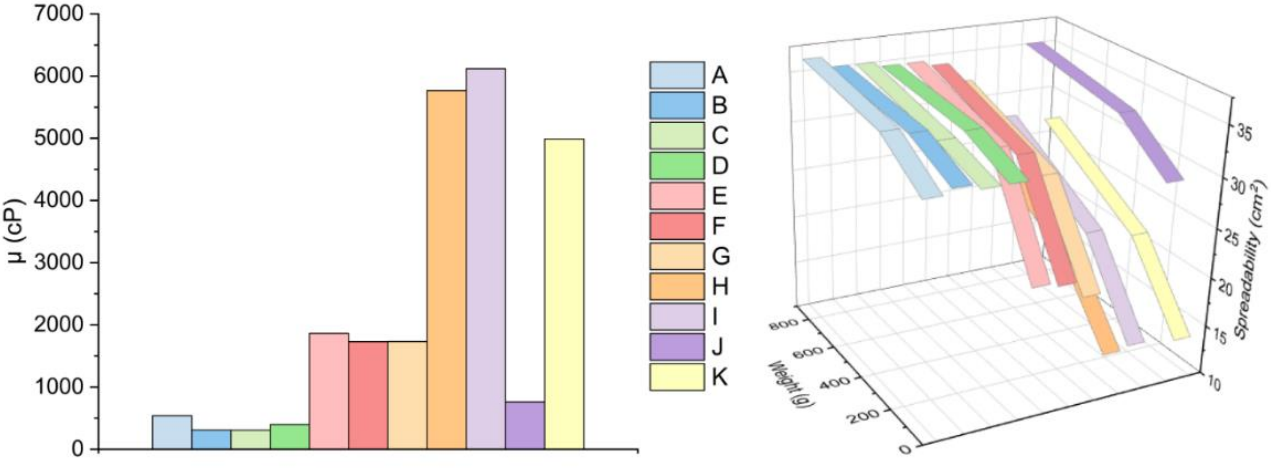

Figure 3.1. Viscosity (left) and spreadability (right) of the different hydrogel formulations.

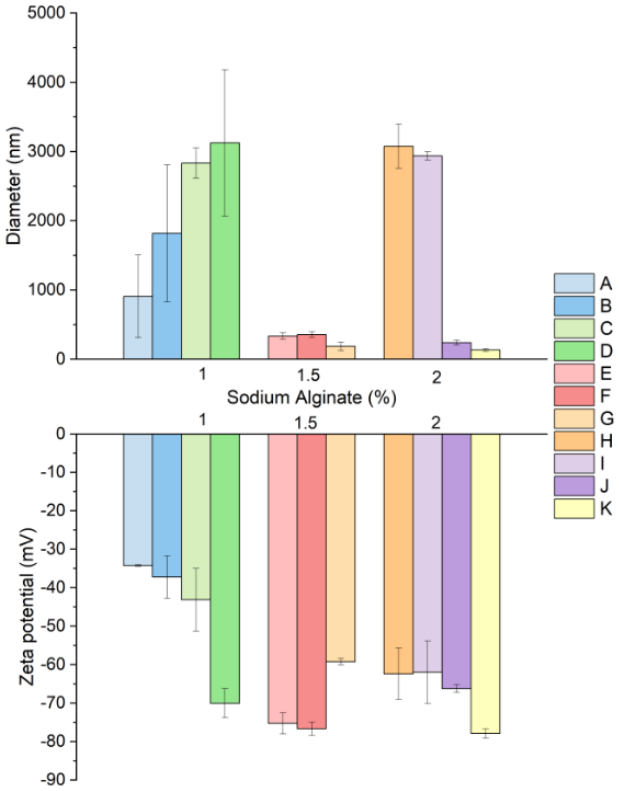

Figure 3.2. Mean particles size (top) and zeta potential (bottom) of the different hydrogel formulations.

3.3.3. Experimental design

To better understand the relation between the independent variables and the rheological properties, the results presented in the previous section were correlated in the *Statistica* program. The p-value test assesses the evidence for the null hypothesis, which corresponds to a statistical theory that suggests that no statistical relationship and significance exists in a set of measured phenomena. If the p-value is less than 0.05, it means strong evidence against the null hypothesis, and thus suggests a statistical and significance relationship between the variables. On the other hand, if the p-value is greater than 0.05, there is, at least, 5% chance of the null hypothesis being correct, and thus the independent variable is not statistically significant.

The F-statistic test is also useful to corroborate with the p-value test. To reject the null hypothesis, considering that an independent variable is statistically significant, the F-values must be high.

3.3.3.1. Viscosity

Regarding the hydrogel viscosity, the results given by the program are shown in figures 3.3 and 3.4. The results presented in figure 3.3 demonstrate that sodium alginate is the independent variable that most contributes for the outcome of viscosity. The concentration of sodium alginate is the only variable surpassing a p-value of 0.5, which is in accordance with the results showed in the ANOVA variance table, where the F-value is bigger than the others and the p-value is less than 0.05. These results suggest that the concentration of sodium alginate is statistically significant in the viscosity of

the hydrogel. In Figure 3.4 it is presented a graphic with the observed versus predicted values for the viscosity of the hydrogel. The value of $R^2 = 0.7998$ is not acceptable for a linear model, which means the data is considered non-linear and the model cannot predict viscosity values in function of the independent variables.

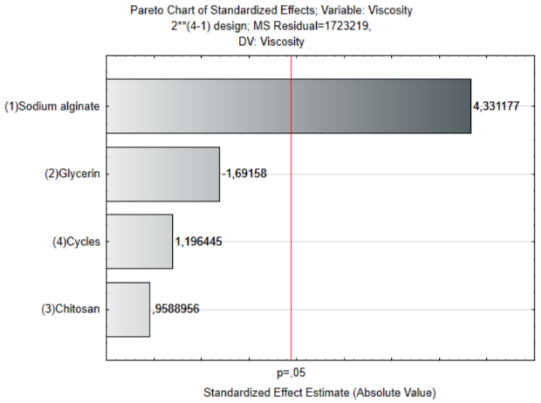

Factor	F	P
Sodium Alginate	18.75909	0.004922
Glycerin	2.86145	0.141677
Chitosan	0.91948	0.374640
Cycles	1.43148	0.276652

Figure 3.3. Pareto chart (left) and analysis table of ANOVA variation for the viscosity of the hydrogel.

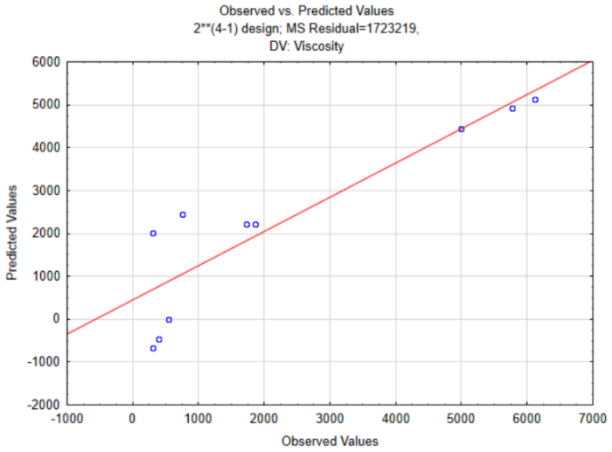

Figure 3.4. Observed and Predict values graphic for viscosity as dependent variable, R^2=0.7998.

Since that the concentration of sodium alginate (structure in figure 3.5) is statistically significant for the viscosity, is important to understand the influence of other variables, such as the number of freeze-thawing cycles and the concentration of glycerine. To analyse these correlations, a fitted surface graphic of the viscosity and the three independent values is shown in Figure 3.6.

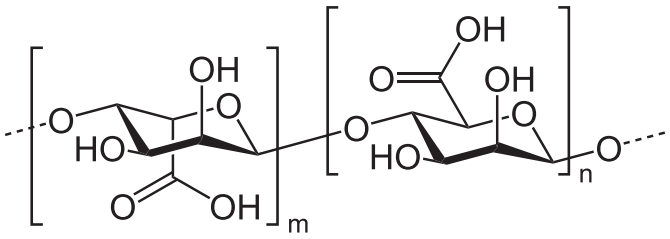

Figure 3.5. Structure of sodium alginate.

In figure 3.6 is possible to see that viscosity slightly increased with the increase in the number of freeze-thawing cycles, which are expected to make crosslinking reactions with water and PVA (structure in figure 3.7), increasing the consistency of the formulation. This phenomenon occurs due to the formation of semi crystalline structures and, consequently, gelation of the hydrogel. The number of freeze-thawing cycles does not have more impact in the viscosity because the concentration of PVA, which is 2%, is a fixed parameter in all formulations. Therefore, the relation between the viscosity and this independent variable is not so obvious. Regarding to glycerine (structure in figure 3.8), with the increase of its concentration, the viscosity of the hydrogel decreases. This relation between the two variables was expected, because glycerine is expected to act as an emollient in the hydrogel.

In terms of the effect of sodium alginate, the viscosity of the hydrogel increases with the increase in its concentration, which is in accordance with the previously results.

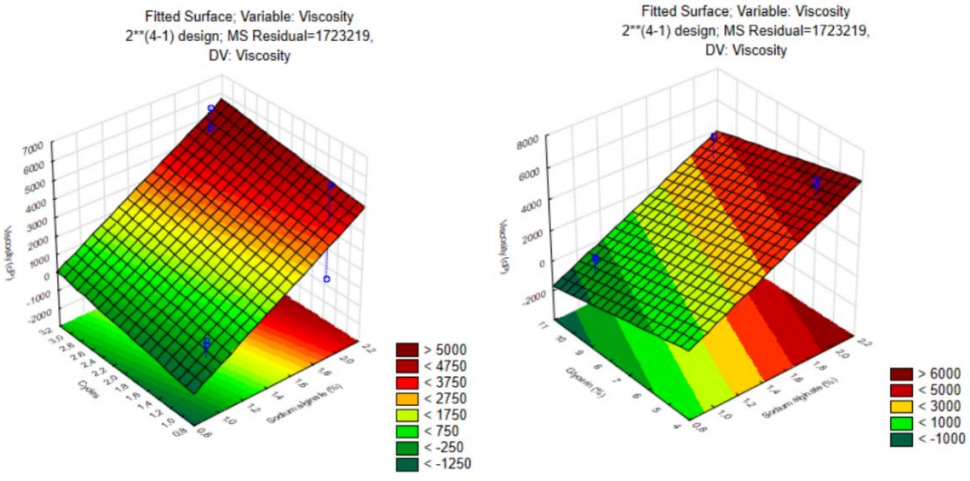

Figure 3.6. Fitted surface graphic for viscosity and sodium alginate concentration with freeze-thawing cycles (left) and glycerine (right).

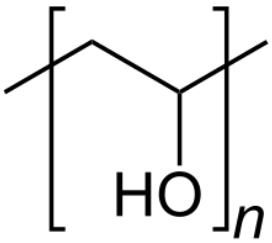

Figure 3.7. Poly(vinyl) alcohol (PVA) structure.

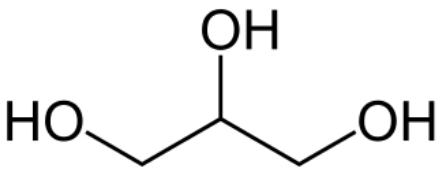

Figure 3.8. Glycerine structure.

3.3.3.2. Spreadability

Regarding the hydrogel spreadability, the results given by the program are shown in Figures 3.9 and 3.10. The results showed in Figure 3.6 reveal that the concentration of sodium alginate is the only variable that can be considered statistically significant for the spreadability. Once more, sodium alginate is the only variable which surpasses a p-value of 0.5 in the pareto chart. The results presented in the ANOVA variance table confirm this relation, since the F-value associated with the independent variable is greater than the others, and the p-value is less than 0.05. Therefore, the concentration of sodium alginate is statistically significant to spreadability.

The results showed in Figure 3.9 reveal that the concentration of sodium alginate is the only variable that can be considered statistically significant for the spreadability. Once more, sodium alginate is the only variable which surpasses a p-value of 0.5 in the pareto chart. The results presented in the ANOVA variance table confirm this relation, since the F-value associated with the independent variable is greater than the others, and the p-value is less than 0.05. Therefore, the concentration of sodium alginate is statistically significant to spreadability. In Figure 3.10 it is presented a graphic with the observed versus predicted values for the spreadability of the hydrogel. Once again, the value of $R^2 = 0.757$ is not acceptable for a linear model, which means the data is considered non-linear and the model cannot predict spreadability values based on the independent variables.

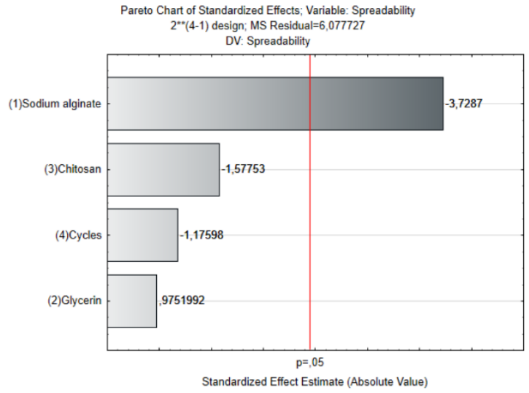

Factor	F	P
Sodium Alginate	13.90322	0.009752
Glycerin	0.95101	0.367123
Chitosan	2.48859	0.165749
Cycles	1.38292	0.284147

Figure 3.9. Pareto chart (left) and analysis table of ANOVA variation for the spreadability of the hydrogel.

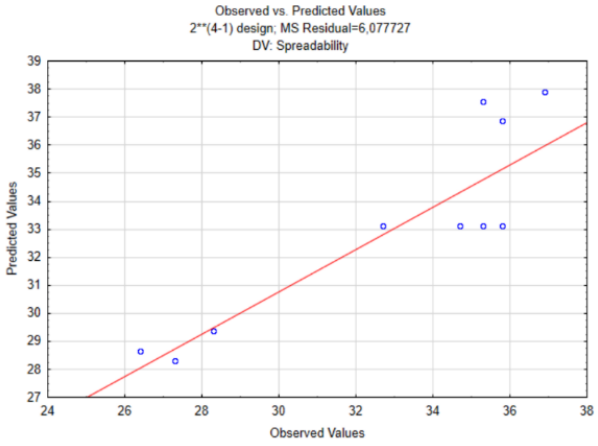

Figure 3.10. Observed and Predict values graphic for spreadability as dependent variable, R^2=0.757.

Since that the concentration of sodium alginate is statistically significant for the viscosity, is important to understand the influence of other variables, such as the number of freeze-thawing cycles and the chitosan concentration. To understand these correlations, a fitted surface graphic of the viscosity and the three independent values is shown in figure 3.11.

Regarding to freeze-thawing, spreadability slightly decreases with the increase in the number of freeze-thawing cycles. The increase of chitosan concentration also promotes a slightly decrease of spreadability. This result is in accordance with the one obtained for the viscosity, since the two dependent variables have a relation already explained. In terms of the effect of sodium alginate, the spreadability of the hydrogel decreases with the increase in its concentration, which is also expected regarding the results obtained for viscosity.

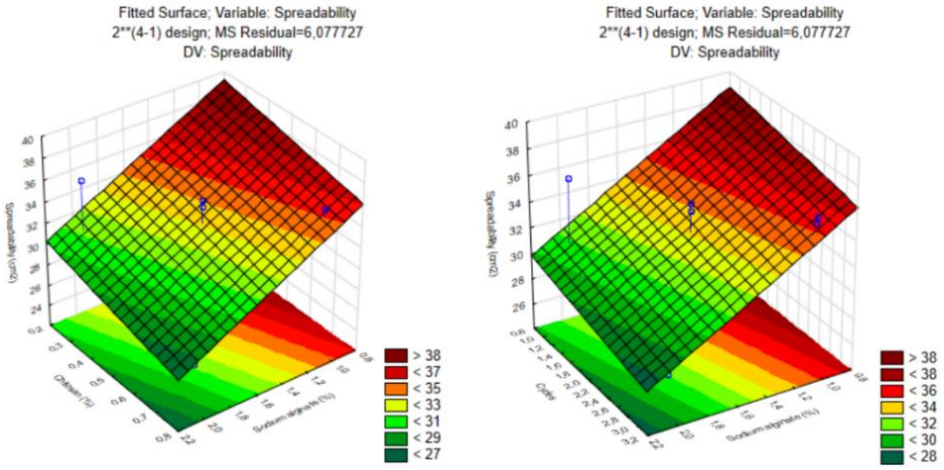

Figure 3.11. Fitted surface graphic for spreadability and sodium alginate concentration with chitosan (left) and freeze-thawing cycles (right).

3.3.3.3. Mean particle size

In terms of mean particle size, the results given by the program are shown in Figures 3.12 and 3.13. The results showed in Figure 3.12 reveal that these independent variables are not statistically significant for the mean particle size. In the pareto chart, none of p-values is equal or greater than 0.5, which is in accordance with the results presented in the ANOVA variance table. Therefore, all the results suggest that the independent variables are not statistically significance for the mean particle size. In Figure 3.13 it is presented a graphic with the observed versus predicted values for the mean particle size. The value of $R^2 = 0.09$ is too low, which means the data is considered non-linear and the model cannot predict the mean particle size based on the independent variables.

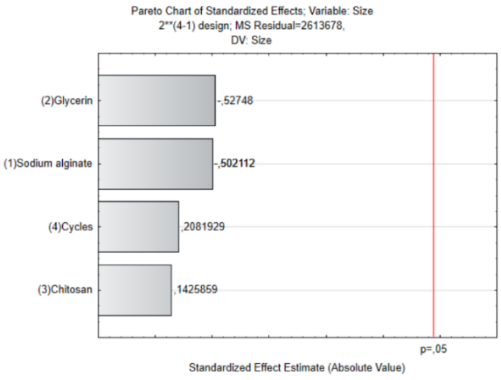

Factor	F	P
Sodium Alginate	0.252117	0.633479
Glycerin	0.278235	0.616787
Chitosan	0.020331	0.891285
Cycles	0.043344	0.841966

Figure 3.12. Pareto chart (left) and analysis table of ANOVA variation for the mean particle size of the hydrogel.

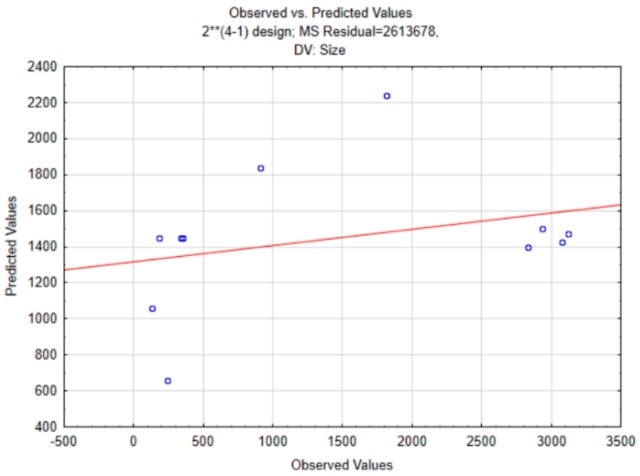

Figure 3.13. Observed and Predict values graphic for mean particle size as dependent variable, R^2=0.09.

3.3.3.4. Zeta Potential

Regarding to zeta potential, the results given by the program are shown in Figures 3.14 and 3.15. The results presented in figure 3.14 reveal that sodium alginate is the only independent variable that can be considered statistically significant for the zeta potential. This independent variable is the only reaching a p-value of 0.5, which is in accordance with the results showed in the ANOVA variance table, where the F-value is the greatest one and the p-value is less than 0.05. These results suggest that the concentration of sodium alginate is statistically significant for the zeta potential. In Figure 3.15 it is presented a graphic with the observed versus predicted values for zeta potential. The data is considered non-linear because of the value of R^2 = 0.646, which is not acceptable for a linear model. Therefore, it is possible to conclude that the model cannot predict zeta potential values in function of the independent variables.

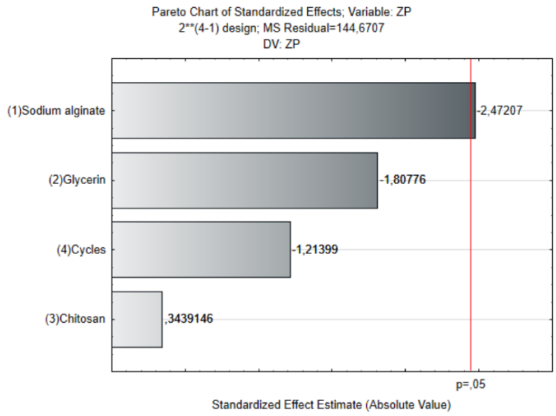

Factor	F	P
Sodium Alginate	6.111129	0.048322
Glycerin	3.267982	0.120649
Chitosan	0.118277	0.742643
Cycles	1.473770	0.270363

Figure 3.14. Pareto chart (left) and analysis table of ANOVA variation for the zeta potential.

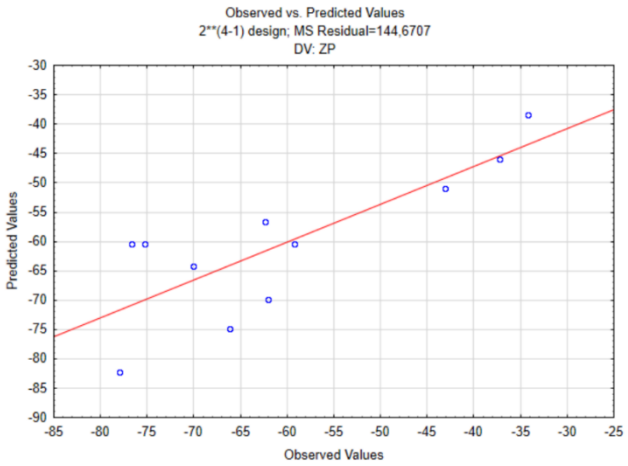

Figure 3.15. Observed and Predict values graphic for zeta potential as dependent variable, R^2=0.646.

Since chitosan (structure in figure 3.16) is positively charged and the concentration of sodium alginate is statistically significant for the zeta potential, it could be important to analyse the fitted surface graphic of these variables, which is showed in figure 3.17. By looking at Figure 3.17 is possible to understand that with the increase of chitosan concentration the zeta potential slightly increases, which is to be expected since chitosan has a positive charge. The effect of chitosan concentration on zeta potential is not more evident because this charge effect is already masked by sodium alginate that is negative charged. When it comes to alginate, the zeta potential decreases with the increase in its concentration, which is in accordance with the results previously mentioned.

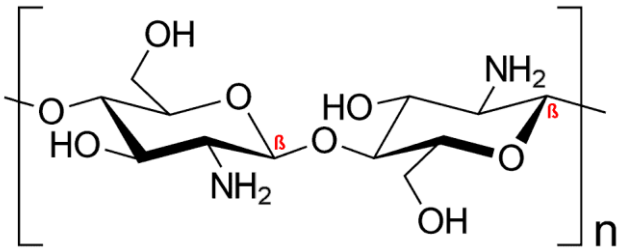

Figure 3.16. Chitosan structure.

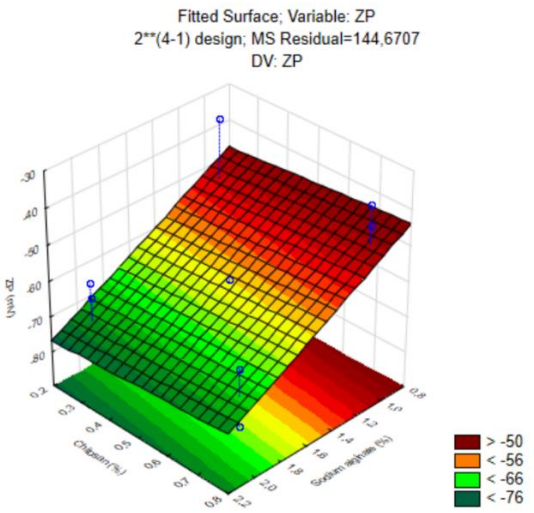

Figure 3.17. Fitted surface graphic for zeta potential dependent variable and sodium alginate concentration with chitosan.

3.3.4. Ideal formulation

With the aim of find the ideal formulation, constraints were established for each variable and given to the Design-Expert program. Since alginate is able of absorbing wound exudate and restricting bacterial infections at the wound site, it was important to maximize its concentration, and a maximum of 2% was established. Regarding to chitosan, which has muco-adhesive properties, it was maintained in the range of 0.25-0.75%. For glycerine, it was established a range between 5-10% in order to maintain, specially, the viscosity of the hydrogel. The number of freeze-thawing cycles was set to just one cycles because it was proven that this variable had not significance for the dependent variables.

In terms of dependent variables, the main goal was to keep the viscosity in the range of 1,000-10,000 cP and the spreadability between the results previously obtained. For the mean particle size and zeta potential, it was established the goal of keep the results in range.

Finally, according with the program, the ideal formulation for the hydrogel would have 2% sodium alginate, 0.75% chitosan, 6% glycerine and 1 freeze-thawing cycle. Therefore, this formulation could be suitable to embed the microparticles loaded with insulin.

4. Microfluidics for production of insulin-loaded alginate microparticles

In this chapter the results and discussion regarding the production and characterization of insulin-loaded alginate microparticles obtained by microfluidics is presented. Starting with the materials and methodology used in the preparation of microparticles, where the main goal was to produce particles with spherical shapes and sizes using a microfluidic device. Then, the structure of insulin upon encapsulation will be evaluated and discussed.

4.1. Materials and Methods

4.1.1. Materials

For the microparticles production, it was used Sodium alginate, very low viscosity, from Alfa Aesar (Massachusetts, MA, United States) and recombinant human insulin from Sigma-Aldrich.

For the insulin structure characterization, it was used thioflavin T from Acros organics (Geel, Belgium) and alginate lyase from Sigma-Aldrich.

Different solutions were prepared with different reagents, and it was used milli-Q water, produced in-house, as solvent.

4.1.2. Preparation of insulin-loaded alginate microparticles

Insulin-loaded alginate microparticles were produced by microfluidics, using the dripping mode approach. The T-junction microfluidic devices were fabricated in poly(dimethylsiloxane) (PDMS) using a soft-lithography technique. A schematic of the microfluidics device is shown in Figure 4.1. The PDMS layers were then treated with oxygen plasma and were permanently bonded to a glass slide. Two syringe pumps from New Era Pump Systems Inc. (Farmingdale, NY, USA) were used to deliver both the continuous phase and the dispersed phase at a constant flow. Therefore, it was prepared a 30 mg/mL insulin solution in 0.1M HCL, which was added to a 1.2M sodium alginate solution. A 2M sodium alginate solution was also considered. However, the increase in alginate concentration prevented the formation of droplets, due to the increase in viscosity. The method used to produce microparticles with well-defined shapes and sizes was based in [145]. A phase diagram, which is shown in Figure 4.2, was used to find the right dispersed phase according with its capillary number.

To predict the absolute droplet size, both the viscous shear and interfacial tension forces were analytically determined. The method used was based in [145].The droplet diameter can be predicted using the following equation:

$$D = 1 + \frac{1}{3Ca_c} \tag{4.1}$$

Where Ca_c is the capillary number of the continuous phase fluid [145].

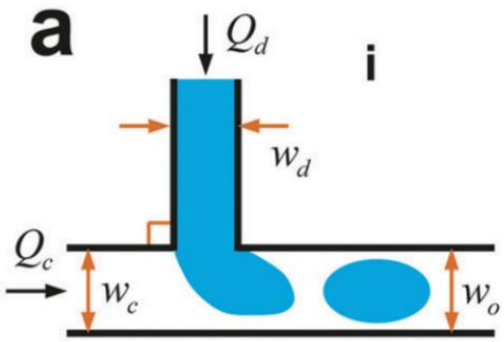

Figure 4.1. Schematic of microfluidics device with "T-junction" where the continuous and dispersed phase fluids meet perpendicularly. Q denote the volumetric flow rate, and w represents the channel diameter. The subscripts "c", "d" and "o" stand for the continuous phase, dispersed phase, and outlet channel, respectively. *Adapted with permission from* [145].

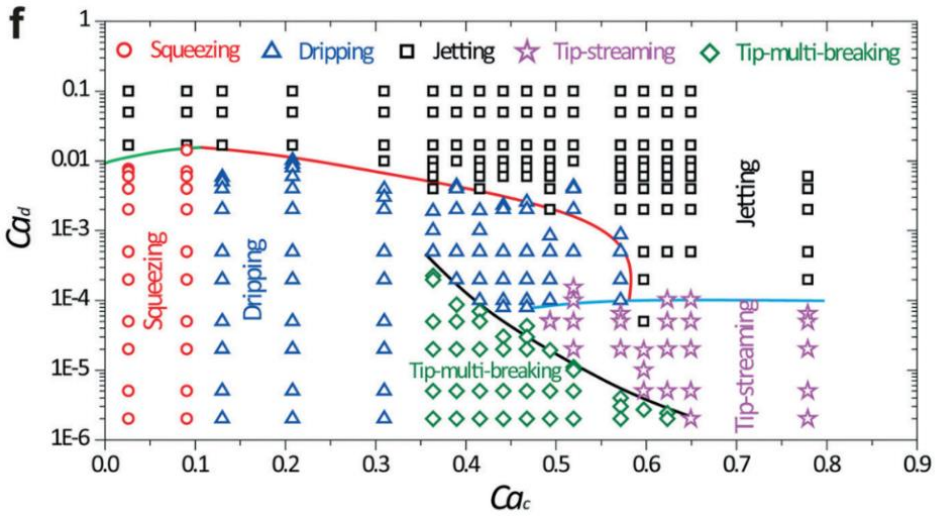

Figure 4.2. Phase diagram in (Cac, Cad) plane for various modes observed in microcapillary flow-focusing devices. *Adapted with permission from* [145].

After production, the microparticles were crosslinked with a 2M Calcium Chloride ($CaCl_2$) solution. Then, the particles were washed by centrifugation for 30min at 11.000 rpm using a Centrifuge 5810 R from Eppendorf International (Hamburg, Germany) and redispersed in 8 mL of PVA 5%(w/v). As control, unloaded alginate microparticles were also prepared. The hydrogel to consider in this chapter is composed of 4% (w/v) PVA, crosslinked with 1%(w/v) sodium tetraborate (TBS).

It is well known that TBS (structure in figure 4.3), also called borax, readily crosslinks PVA via di-diol complexation formed between two adjacent diol groups from PVA and TBS [159]. This two-step procedure starts with an initial mono-diol complexation, which produces a poly(electrolyte) and, as a result of electrostatic repulsion, causes the expansion of individual polymer chains, producing a favourable environment for the proceeding di-diol complexation reaction to occur [160]. When the existing inter-molecular cross-links is sufficient, the network takes the form of a gel [158].

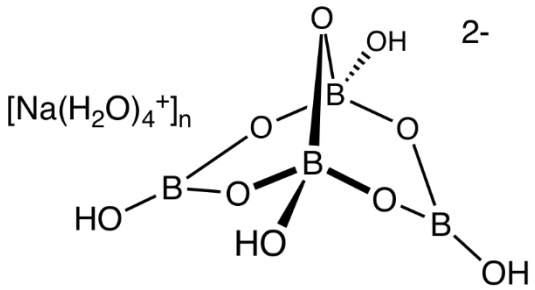

Figure 4.3. Sodium tetraborate (TBS) structure.

4.1.3. Microparticle characterization

4.1.3.1. Scanning electron microscopy

Characterization of the insulin-loaded alginate microparticles surface morphology, upon freeze-drying, was assessed by scanning electron microscopy (SEM) with an Analytical FEG-SEM: JEOL 7001F microscope from Jeol Ltd. (Tokyo, Japan). The microparticles were analysed after lyophilization, as well as after production and prior to lyophilization. All samples were treated onto metal stubs and vacuum-coated with a layer of gold/palladium before SEM microscope observation.

4.1.3.2. Insulin in vitro release study

To study the insulin release profile, cell culture inserts from Thermo Fisher Scientific with 8 µm pore size were used. The polycarbonate membrane which is present in each off the inserts allows soluble material to pass to into the receiver compartment. Samples with around 1g of hydrogel with insulin-loaded microparticles were placed in the inserts, which were suspended in 5 mL of pH 7.4 PBS solution and incubated at 37°C under stirring at 150 rpm. Samples were taken at predetermined time intervals of 0.5, 1, 2, 4, 8, 24 and 48 hours and fresh medium at the same temperature was replaced to keep the initial volume. The collected samples were then centrifuged at 13,000 rpm for 30 minutes, and the content of insulin supernatant was determined by Nanodrop. All samples were run in triplicate**.**

4.1.4. Insulin structural characterization

4.1.4.1. Insulin extraction

Microparticle samples, previously frozen at -80°C, were lyophilized for 48h, with a Scanvac Cool Safe from LaboGene (Lillerød, Denmark). Microparticles were freeze-dried without cryoprotectant and added with trehalose at a cryoprotectant concentration of 5% (w/v). To release the insulin, the lyophilized particles were submitted to 500 µL of 0.1M alginate lyase aqueous solution. The mixture was centrifuge at 5000 rpm for 5 minutes, and the content was submitted to protein structure analysis.

4.1.4.2. Circular dichroism analysis

The secondary structure of the extracted insulin was assessed by Circular Dichroism (CD), using an π^*-180 spectrometer from Applied Photophysics (Leatherhead, UK) and Pistar software. The lamp housing was continuously purged with nitrogen at a flow of 8mL/min at 25°C, and the control protein spectrum was obtained using a 0.2mg/mL solution of insulin in 0.01M HCL. All the experiments were collected from an average of 3 scans in the 190-250 nm region, using an averaging time of 1 s, with a step of 0.5 nm. The signal was then converted to molar ellipticity using the following equation:

$$\theta = \frac{CD\ signal \times MRW}{10 \times cell\ path\ lenght \times insulin\ concentration} \quad (4.2)$$

Where MRW represents the mean residual weight of each insulin residue 116 (Da). The insulin concentration was determined by UV absorption at 280 nm, using a NanoDrop ND-1000 Spectrophotometer from Thermo Fisher Scientific (Waltham, EUA), with a molar extinction coefficient of 5800 $M^{-1}cm^{-1}$.

4.1.4.3. Fluorescence spectroscopy analysis

The tertiary structure of the extracted protein was studied using fluorescence emission spectra, obtained with a Cary Eclipse Fluorescence Spectrophotometer, from Varian, Inc (Palo Alto, USA), in a 260-400 nm range with 1 nm step, and excitation occurring at 280 nm. It was used an averaging time of 0.1 s and emission/excitation slits at 10 nm. The reference spectrum, which was auto subtracted from the samples' spectra, was obtained using a 0.01M HCL solution and the control protein spectrum using a 0.2 mg/mL solution of insulin in 0.01M HCL.

4.1.4.4. Thioflavin T assay

The extracted protein was also used to perform a thioflavin T assay, in order to assess the existence of insulin fibrillation, which is an indicator or protein denaturation. The experiments were performed with a Cary Eclipse Fluorescence Spectrophotometer from Varian, Inc (Palo Alto, USA), using a thioflavin T concentration of 25 µM and insulin concentration of about 11 µM. The samples were excited at 450 nm, the intensity was measured at 485 nm with slit widths at 5nm, and it was used an averaging time of 0.1 s. The negative control consisted of a fresh 0.2 mg/mL solution of insulin in 0.01M HCL, and the positive control of a 0.2 mg/mL insulin solution heated at 60ºC.

4.1.4.5. Fourier Transform Infrared Spectroscopy

The secondary structure of insulin loaded into alginate microparticles was also assessed by Fourier Transform Infrared Spectroscopy (FTIR). The spectra were collected with a Spectrum Two from PerkinElmer (Waltham, MA, USA) equipped with an attenuated total reflectance (ATR). All spectra were collected with 256 scans and a $4cm^{-1}$ resolution in the region of 4000-600 cm^{-1}. All

formulations were run in triplicates, and the result here presented corresponds to the average. All spectra were area-normalized for further comparison.

4.2. Results and Discussion

4.2.1. Microparticle Characterization

4.2.1.1. Scanning Electronic Microscopy

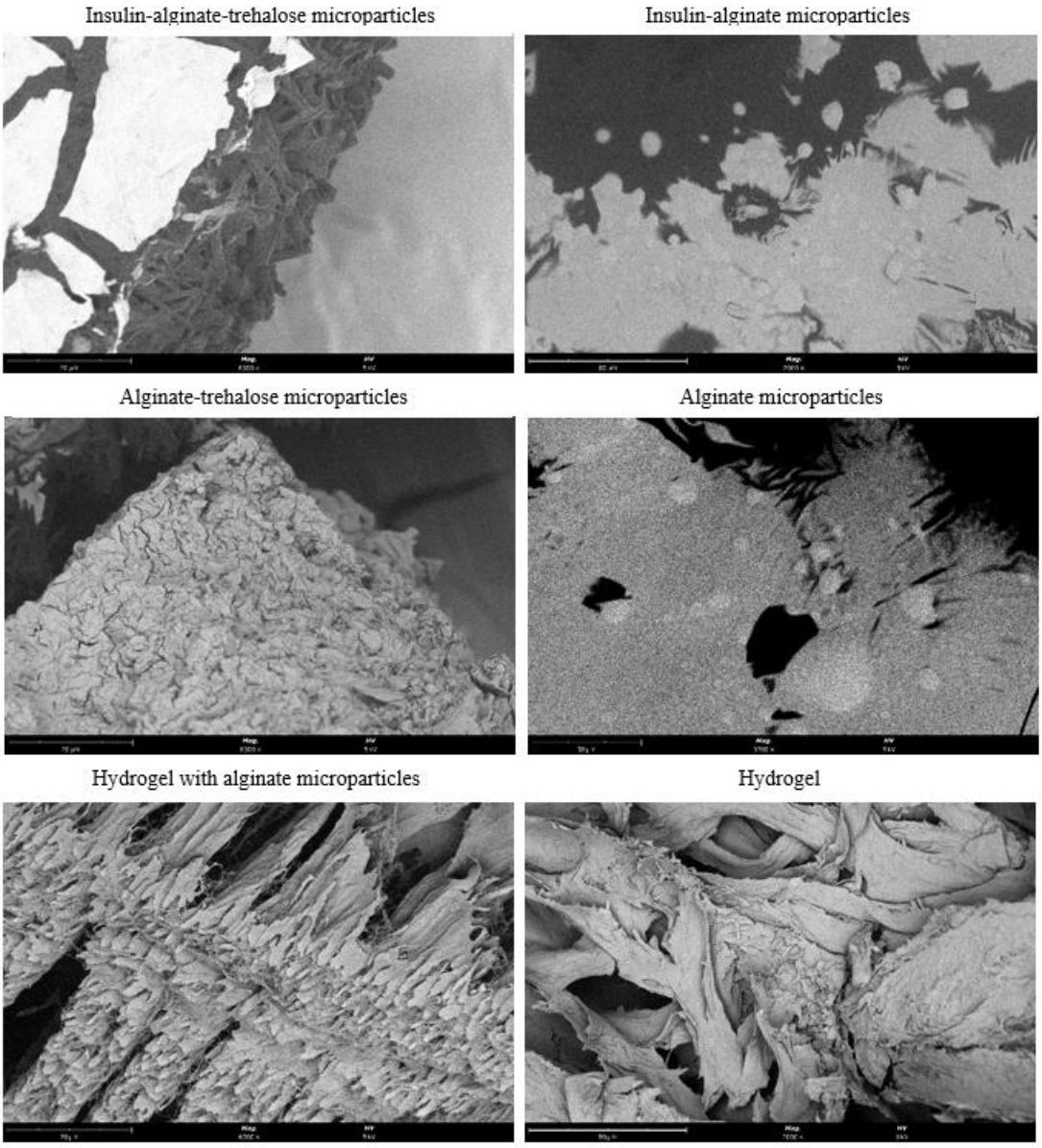

Figure 4.4. Microparticles-hydrogel SEM images. Insulin-loaded alginate microparticles with cryoprotectant, alginate microparticles with cryoprotectant, insulin-loaded alginate microparticles, alginate microparticles, hydrogel with and without microparticles (from top to bottom). Scale bar: 20 µm for pictures of the first column, 80 µm for the first picture of the second column, 30 µm for the second picture of the second column, and 50 µm for the third picture of the second column.

To assess the physiognomy of the microparticles and the hydrogel, SEM images were obtained (Figure 4.4). Regarding the microparticles without cryoprotectant, it is not possible to see significant differences between those with and without insulin, which confirms that insulin encapsulation does not change the physiognomy.

4.2.1.2. In vitro Insulin Release

In Figure 4.5, it is shown the cumulative release profile of insulin from microparticles embedded into the hydrogel in 48h. The release profile obtained is characterized by an initial burst release within the first 4 hours and a sustained release pattern until the 48h.This initial burst release can be related with the fraction of insulin that remained adsorbed on the microparticle surface, facilitating the diffusion to the medium. From that moment on, a sustained release pattern is observed until the 48h, reaching around 22%. The prolonged release can be attributed to the slow diffusion of the medium, which allows a sustained insulin release. The release profile suggests that insulin is probably distributed within the particle instead of having a preferential deposition. If the hydrogel was not present, the microparticles would be able to release the insulin more easily. However, the hydrogel creates a barrier for the release of insulin, because the microparticles are embedded into the matrix, which allows a more controlled and sustained release.

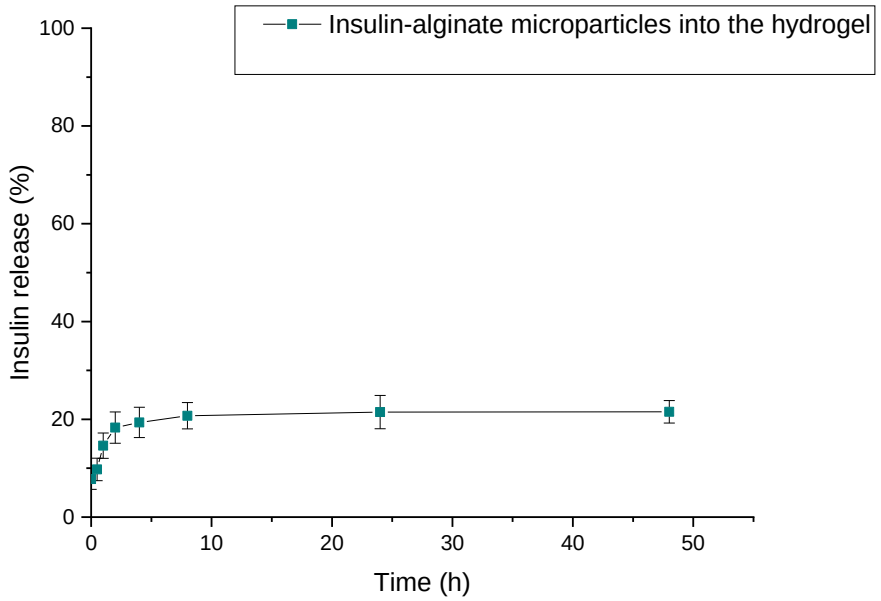

Figure 4.5. Insulin release profile from insulin-loaded microparticles.

4.2.2. Protein Structure

To perform the insulin extraction, the microparticles previously frozen at -80°C, were lyophilized for 48h, both with and without cryoprotectant. In Figure 4.6 photos of the different formulations upon lyophilization are shown.

Figure 4.6. Photos of the different microparticles upon lyophilization. From left to right: insulin microparticles, insulin-trehalose microparticles, alginate microparticles, alginate-trehalose microparticles.

4.2.2.1. Circular Dichroism

The success of a protein-loaded delivery system depends on the maintenance of protein structure and consequently its bioactivity. Therefore, after particle production and incorporation into the hydrogel, the secondary structure of insulin was analysed by Circular Dichroism (CD). CD spectroscopy consists of the use of circularly polarized light to study the conformation of asymmetrical molecules. Usually, the secondary structure (α-helix and β-sheet) can predict the efficacy of insulin [161]. Since proteins absorb right- and left-circularly polarized light differently according to their optical activity, it is possible to probe insulin's secondary structure with CD spectra [162]. The spectra obtained are shown if Figure 4.7.

The spectra used as reference corresponds to a fresh solution of insulin at 0.2 mg/mL, resulting in a spectrum with two ellipticity minimum, characteristic of the predominant α-helical structure of the protein, at 208 nm and 221,5 nm [163]. A maximum was also observed at 194 nm, which is in accordance with other described in previous works.

The structural modification that can lead to denaturation, aggregation or fibrillation is evidenced by prevalent β-sheet content, and an ellipticity minimum occurs around 216 nm [164]. Since this is not observed in the sample spectra, the structural modification from α-helix to β-sheet did not occur and is possible to conclude that the insulin extracted from the microparticles maintained its secondary structure. However, there is a decrease of the negative ellipticity signal, which demonstrate some changes in the spatial conformation of the protein upon lyophilization. These differences observed in the spectra are related to the ellipticity signal and can be explained with the exposure to invasive procedures, such as the extraction of insulin from the microparticles. No significant differences were found between the insulin spectra from microparticles with and without cryoprotectant.

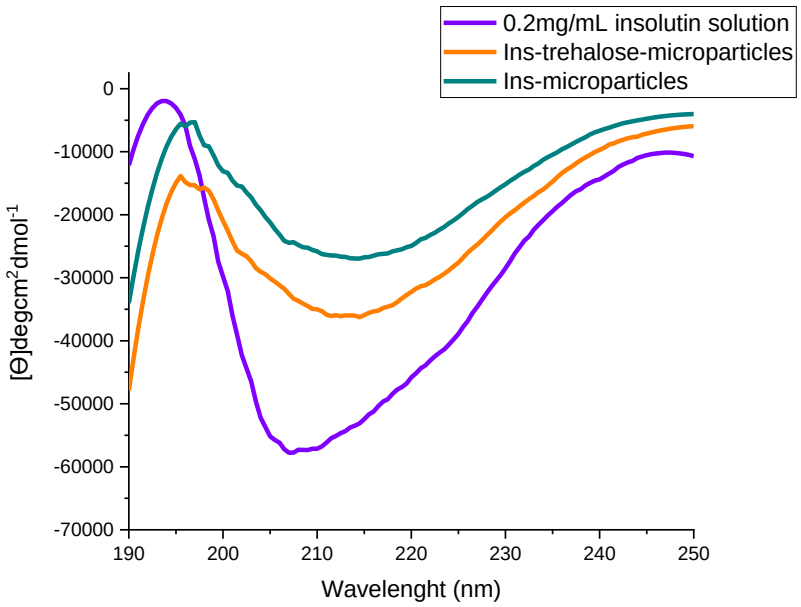

Figure 4.7. Far-UV CD spectra of insulin extracted from insulin-loaded alginate microparticles lyophilized with and without cryoprotectant. Insulin 0.2 mg/mL in 0.01 HCL used as reference.

4.2.2.2. Fluorescence Spectroscopy

Tertiary structure of extracted insulin was assessed by fluorescence spectroscopy. Since insulin lacks tryptophan, the protein fluorescence depends mostly in the four tyrosine residues. The modification of the emission spectra of insulin fluorescence is an indicator of possible changes in protein structure. Structural modifications related to insulin denaturation, aggregation or fibrillation are characterized by a decrease in the intensity of fluorescence emission and the shift of its maximum.

An insulin solution at 0.2 mg/ml was used to obtain the reference insulin spectrum. In this spectrum, the maximum was observed at 285 nm. This maximum is shifted when compared to the literature, where the maximum fluorescence intensity is evidenced at 304 nm [96]. When comparing the sample spectra with the spectrum of native insulin (Figure 4.8.), there is a slightly decrease in the intensity of fluorescence emission and a slightly shift of its maxima. Since the spectra are quite similar, it is possible to conclude that minimal structural modifications occur. These results might be a consequence of the stress exposure of the insulin during the extraction from the microparticles, and lyophilization process. Regarding these results, it is possible to conclude that the structure of insulin and, consequently, its bioactivity were maintained upon encapsulation. No significant differences were found between the insulin spectra from microparticles with and without cryoprotectant.

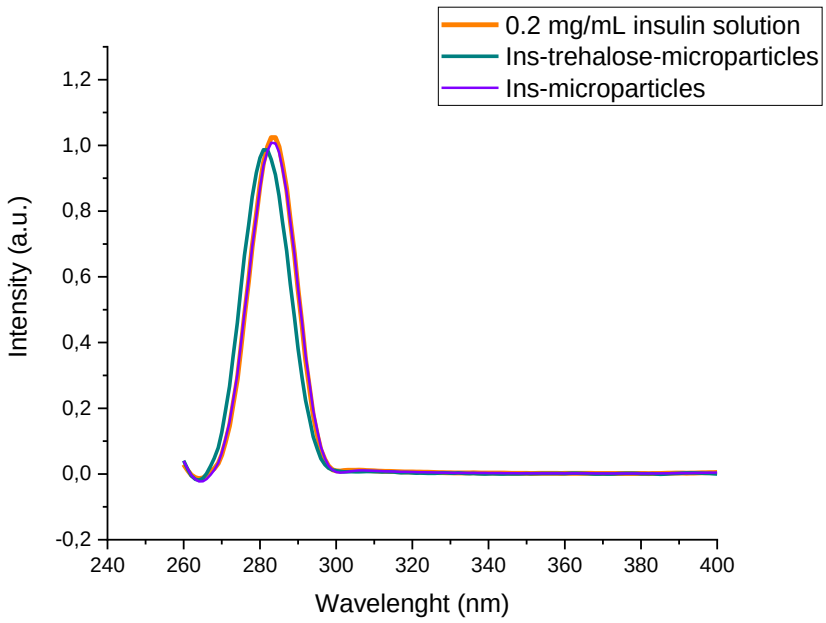

Figure 4.8. Fluorescence spectra of insulin extracted from insulin-loaded alginate microparticles lyophilized with and without microparticles. Insulin 0.2mg/mL in 0.01 HCL used as reference.

4.2.2.3. Thioflavin T assay

The thioflavin T assay was used to assess the fibrillation of insulin, which is a signal of possible denaturation. The presence of amyloid fibrils, which are protein aggregates, indicate that protein structure, as well as its bioactivity, are compromised [95]. Thioflavin T is a dye able to bind to those amyloid fibrils, with crossed β-sheet structures, leading to a shift of the fluorescence excitation maximum, and an increase of fluorescence emission at 485 nm [165]. Therefore, the increasement of the thioflavin T fluorescence intensity indicates insulin fibrillation.

No fluorescence emission was detected at 485 nm, which means that insulin extracted from the alginate microparticles did not evidence the presence of amyloid fibrils. In the other hand, the positive control made of fibrillated insulin showed fluorescence emission. Therefore, the encapsulation process and lyophilization did not promote insulin fibrillation, which means the protein maintained its structure.

4.2.2.4. Fourier-Transform Infrared Spectroscopy

ATR-FTIR spectroscopy is one of the most useful techniques due to its ability to assess encapsulated protein's secondary structure in a non-invasive way [166]. In this work, ATR-FTIR spectroscopy was used to study the interactions between the components of the microparticles. The samples analysed were the microparticles both with and without insulin. Spectra are shown in Figure 4.9. The region of 1710-1590 cm^{-1} (amide I) is the most representative region of the insulin spectra.

Modification of α-helix band, which is the major component of the amide I spectrum, are the most characteristic of protein denaturation and consequent loss of activity [161].

From figure 4.9 is possible to see that the spectra from alginate microparticles loaded with insulin is very similar to the spectra from unloaded microparticles, which means that the interactions between the polymer and the protein are not evident. The spectral region of amide I (1710-1590 cm^{-1}) is slightly different in the spectrum of insulin loaded microparticles, where is possible to see two peaks at 1653 and 1630 cm^{-1}, which supports the presence of insulin in the microparticles.

Stretching vibrations of O-H bonds of alginate appear in the range of 3000-3600 cm^{-1} are representative of the sodium alginate spectrum. Stretching vibrations of C-H are also commonly observed at 2920-2850 cm^{-1}. Bands in 1649 and 1460 cm^{-1} can also be considered and are attributed to asymmetric and symmetric stretching vibrations of carboxylate salt ion, respectively. In figure 4.9 is possible to see the presence of these bands, which are characteristic of the native polymer spectrum and support the results already reported.

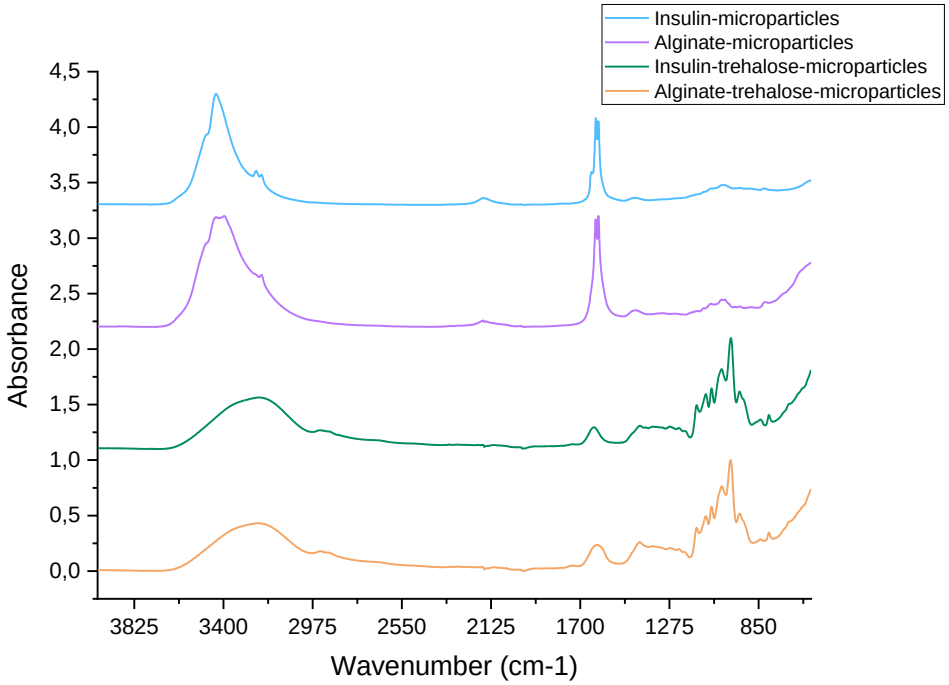

Figure 4.9. Normalised FTIR spectra of alginate microparticles, with and without insulin, lyophilized with and without cryoprotectant.

5.Conclusion and future perspectives

This research was divided in two parts, both important to the development of a new delivery system consisting of a hydrogel with microparticles encapsulating insulin by microfluidics, for wound healing applications.

Regarding the hydrogel production and characterization, it was possible to understand how the concentration of chitosan, alginate and glycerine, as well as the number of freeze-thawing cycles influenced que properties of the hydrogel, such as viscosity and spreadability. The concentration of sodium alginate in the formulation was the parameter with more influence in the hydrogel properties. Finally, it was found that the optimal formulation corresponds to a hydrogel with 2% alginate, 6% glycerine, 0.75% chitosan and 1 freeze-thawing cycle, suitable for topical application.

Stepping into the second phase of this work, it was possible to produce spherical alginate microparticles loaded with insulin, using a droplet-based microfluidics approach. The results obtained after insulin extraction demonstrated that the peptide hormone maintained its structure upon encapsulation, with the presence of minimal alterations. The results concerning the insulin release profile revealed a sustained and controlled release of the protein for 48 hours, suggesting a maintenance of these conditions even after this period.

On balance, the objectives proposed for this thesis were achieved. First, it was possible to find the optimal formulation of the hydrogel, and then encapsulate insulin into microparticles following an approach that allowed the preservation of its structure.

Since it was not possible to co-encapsulate the MSCs, it is important to mention the necessity of continuing this research. Therefore, the next step starts with the co-encapsulation of MSCs together with insulin. Then, it is important to evaluate the MSCs viability upon encapsulations and perform studies to evaluate the cytotoxicity profile of the formulations, as well as its bioactivity. Finally, after performing *in vitro* in *in vivo* testing, it is expected to obtain a delivery system consisting of a hydrogel incorporating microparticles co-encapsulating insulin and MSCs for wound healing applications.

References

1. Sen, C.K., *Human wounds and its burden: An updated compendium of estimates.* Advances in Wound Care, 2019. **8**(2): p. 39-48.
2. Järbrink, K., et al., *The humanistic and economic burden of chronic wounds: a protocol for a systematic review.* Systematic reviews 2017. **6**(1): p. 1-7.
3. Phillips, C.J., et al., *Estimating the costs associated with the management of patients with chronic wounds using linked routine data.* International Wound Journal, 2016. **13**(6): p. 1193-1197.
4. Macedo, A.S., et al., *Nanocarrier-Mediated Topical Insulin Delivery for Wound Healing.* Materials 2021. **14**(15): p. 4257.
5. Menke, N.B., et al., *Impaired wound healing.* Clinics in Dermatology, 2007. **25**(1): p. 19-25.
6. Besson, J.C.F., et al., *Insulin complexed with cyclodextrins stimulates epithelialization and neovascularization of skin wound healing in rats.* Injury, 2017. **48**(11): p. 2417-2425.
7. Lai-Cheong, J.E. and J.A. McGrath, *Structure and function of skin, hair and nails.* Medicine, 2013. **41**(6): p. 317-320.
8. Gallo, R.L. and V. Nizet, *Innate barriers against skin infection and associated disorders.* Drug Discovery Today: Disease Mechanisms, 2008. **5**(2): p. 145-152.
9. Kanitakis, J., *Anatomy, histology and immunohistochemistry of normal human skin.* European Journal of Dermatology, 2002. **12**: p. 390-399.
10. Losquadro, W.D., *Anatomy of the Skin and the Pathogenesis of Nonmelanoma Skin Cancer.* Facial Plastic Surgery Clinics of North America, 2017. **25**(3): p. 283-289.
11. Yousef, H., M. Alhajj, and S. Sharma, Anatomy. Skin (Integument), Epidermis. In: *StatPearls*. Treasure Island (FL): StatPearls Publishing; November 19, 2021.
12. Webb, A., A. Li, and P. Kaur, *Location and phenotype of human adult keratinocyte stem cells of the skin.* Differentiation, 2004. **72**(8): p. 387-395.
13. Agarwal, S. and K. Krishnamurthy, *Histology, skin.* 2019.
14. Ita, K., *Chapter 2 - Anatomy of the human skin*, in *Transdermal Drug Delivery*, K. Ita, Editor. 2020, Academic Press. p. 9-18.
15. Murphrey, M.B., J.H. Miao, and P.M. Zito. *Histology,* Stratum Corneum. In: *StatPearls*. Treasure Island (FL) StatPearls Publishing; November 19, 2021.
16. Yurchenco, P.D. and J.C. Schittny, *Molecular architecture of basement membranes.* FASEB Journal, 1990. **4**: p. 1577-1590.
17. Arda, O., N. Göksügür, and Y. Tüzün, *Basic histological structure and functions of facial skin.* Clinics in Dermatology, 2014. **32**(1): p. 3-13.
18. Marcos-Garcés, V., et al., *Age-related dermal collagen changes during development, maturation and ageing - a morphometric and comparative study.* J Anat, 2014. **225**(1): p. 98-108.
19. Abdo, J.M., N.A. Sopko, and S.M. Milner, *The applied anatomy of human skin: A model for regeneration.* Wound Medicine, 2020. **28**: p. 100179.
20. Ita, K.B., *Transdermal drug delivery: progress and challenges.* Journal of Drug Delivery Science and Technology, 2014. **24**: p. 245-250.
21. Smith, M.M. and J. Melrose, *Proteoglycans in Normal and Healing Skin.* Advances in Woud Care, 2015. **4**: p. 152-173.
22. Rodrigues, M., et al., *Wound Healing: A Cellular Perspective.* Physiological Reviews, 2019. **99**: p. 665-706.
23. Kucharzewski, M., et al., *Novel trends in application of stem cells in skin wound healing.* European Journal of Pharmacology, 2019. **843**: p. 307-315.

24. Morton, L.M. and T.J. Phillips, *Wound healing and treating wounds: Differential diagnosis and evaluation of chronic wounds.* Journal of the American Academy of Dermatology, 2016. **74**: p. 589-605.
25. Demidova-Rice, T.N., J.T. Durham, and I.M. Herman, *Wound Healing Angiogenesis: Innovations and Challenges in Acute and Chronic Wound Healing.* Adv Wound Care (New Rochelle), 2012. **1**(1): p. 17-22.
26. Sun, B.K., Z. Siprashvili, and P.A. Khavari, *Advances in skin grafting and treatment of cutaneous wounds.* Science, 2014. **346**: p. 941-945.
27. Wang, P.-H., et al., *Wound healing.* Journal of the Chinese Medical Association, 2018. **81**(2): p. 94-101.
28. Han, G. and R. Ceilley, *Chronic wound healing: A review of current management and treatments.* Advances in Therapy, 2017. **34**: p. 599-610.
29. Las Heras, K., et al., *Chronic wounds: Current status, available strategies and emerging therapeutic solutions.* Journal of Controlled Release, 2020. **328**: p. 532-550.
30. Singh, S., A. Young, and C.-E. McNaught, *The physiology of wound healing.* Surgery (Oxford), 2017. **35**: p. 473-477.
31. Aukhil, I., *Biology of wound healing.* Periodontology 2000, 2000. **22**(1): p. 44-50.
32. Bhushan, M., et al., *Recent advances in cutaneous angiogenesis.* British Journal of Dermatology, 2002. **147**: p. 418-425.
33. Baum, C.L. and C.J. Arpey, *Normal cutaneous wound healing: Clinical correlation with cellular and molecular events.* Dermatologic Surgery, 2005. **31**: p. 674-686.
34. Li, J., J. Chen, and R.S. Kirsner, *Pathophysiology of acute wound healing.* Clinics in Dermatology, 2007. **25**: p. 9-18.
35. Goldberg, S.R. and R.F. Diegelmann, *Wound healing primer.* Surgical Clinics, 2010. **90**(6): p. 1133-1146.
36. Velnar, T., T. Bailey, and V. Smrkolj, *The wound healing process: an overview of the cellular and molecular mechanisms.* Journal of International Medical Research, 2009. **37**(5): p. 1528-1542.
37. Eming, S.A., P. Martin, and M. Tomic-Canic, *Wound repair and regeneration: mechanisms, signaling, and translation.* Science Translational Medicine, 2014. **6**: p. 265-266.
38. Xue, M. and C.J. Jackson, *Extracellular Matrix Reorganization During Wound Healing and Its Impact on Abnormal Scarring.* Advances in wound care, 2015. **4**(3): p. 119-136.
39. Cha, J., et al., *Fibroblasts from non-healing human chronic wounds show decreased expression of βig-h3, a TGF-β inducible protein.* Journal of Dermatological Science, 2008. **50**: p. 15-23.
40. Patel, S., A. Maheshwari, and A. Chandra, *Biomarkers for wound healing and their evaluation.* Journal of Wound Care, 2016. **25**: p. 46-55.
41. Das, S. and A.B. Baker, *Biomaterials and nanotherapeutics for enhancing skin wound healing.* Frontiers in bioengineering and biotechnology, 2016. **4**: p. 82.
42. Reger, S.I., V.K. Ranganathan, and V. Sahgal, *Support surface interface pressure, microenvironment, and the prevalence of pressure ulcers: an analysis of the literature.* Ostomy Wound Manage, 2007. **53**(10): p. 50-58.
43. Reger, S.I. and V.K. Ranganathan, *The importance of the microenvironment of support surfaces in the prevalence of pressure ulcers*, in *Bioengineering Research of Chronic Wounds: A Multidisciplinary Study Approach*, A. Gefen, Editor. 2009, Springer Berlin Heidelberg: Berlin, Heidelberg. p. 85-100.
44. Smith, D.M., et al., *Evaluation of the bacterial diversity of pressure ulcers using bTEFAP pyrosequencing.* BMC medical genomics, 2010. **3**: p. 41.
45. Sørensen, M.L.B., et al., *Healing of diabetic foot ulcers in patients treated at the Copenhagen Wound Healing Center in 1999/2000 and in 2011/2012.* Journal of Diabetes Research, 2019; 2019:6429575. Published 2019 Sep 8.
46. Falanga, V., *Wound healing and its impairment in the diabetic foot.* Lancet, 2005. **366**: p. 1736-1743.

47. Banu, A., et al., *Spectrum of bacteria associated with diabetic foot ulcer and biofilm formation: A prospective study.* The Australasian medical journal, 2015. **8**(9): p. 280-285.
48. Thomas, P.R., G.B. Nash, and J.A. Dormandy, *White cell accumulation in dependent legs of patients with venous hypertension: a possible mechanism for trophic changes in the skin.* British Medical Journal (Clinical Research Edition), 1988. **296**(6638): p. 1693-1695.
49. Pugliese, D.J., *Infection in venous leg ulcers: considerations for optimal management in the elderly.* Drugs & Aging, 2016. **33**(2): p. 87-96.
50. Ikegami, Y., et al., *Heparin-conjugated collagen as a potent growth factor-localizing and stabilizing scaffold for regenerative medicine.* Regenerative Therapy, 2020. **15**: p. 236-242.
51. E. Windmaier, H., K.T. Raff, and S. (Eds.), *Human physiology: the mechanisms of body function*. 9th ed. 2004, New York McGraw-Hill.
52. Hrynyk, M. and R.J. Neufeld, *Insulin and wound healing.* Burns, 2014. **40**(8): p. 1433-1446.
53. Watkins, P.J., *Choice of insulin.* British Medical Journal, 1983. **287**(6405): p. 1571-1572.
54. Ladisch, M.R. and K.L. Kohlmann, *Recombinant human insulin.* Biotechnology Progress, 1992. **8**(6): p. 469-478.
55. Petrides, D., E. Sapidou, and J. Calandranis, *Computer-aided process analysis and economic evaluation for biosynthetic human insulin production—A case study.* Biotechnology and Bioengineering, 1995. **48**(5): p. 529-541.
56. Brem, H. and M. Tomic-Canic, *Cellular and molecular basis of wound healing in diabetes.* Journal of Clinical Investigation, 2007. **117**: p. 1219-1222.
57. Gore, D.C., et al., *Hyperglycemia exacerbates muscle protein catabolism in burn-injured patients.* Critical Care Medicine, 2002. **30**: p. 2438-2442.
58. Van den Berghe, G., *Insulin therapy for the critically ill patient.* Clinical Cornerstone, 2003. **5**(2): p. 56-63.
59. Gurtner, G.C., et al., *Wound repair and regeneration.* Nature, 2008. **453**: p. 314-321.
60. Madibally, S.V., et al., *Influence of insulin therapy on burn wound healing in rats.* Journal of Surgical Research, 2003. **109**: p. 92-100.
61. Kabalak, A.A., A. Ceylan, and C. Vural, *Effect of insulin treatment to systemic inflammatory response in burn injury.* The New England Journal of Medicine 2013. **30**: p. 191-194.
62. Chen, X., X. Zhang, and Y. Liu, *Effect of topical insulin application on wound neutrophil function.* Wounds 2012. **24**(7): p. 178-184.
63. Azevedo, F., et al., *Effect of topical insulin on second-degree burns in diabetic rats.* Biological Research for Nursing, 2016. **18**: p. 181-192.
64. Zhang, X.-j., et al., *Local injection of insulin-zinc stimulates DNA synthesis in skin donor site wound.* Wound Repair and Regeneration, 2007. **15**(2): p. 258-265.
65. Li, X., et al., *Functionalized silk fibroin dressing with topical bioactive insulin release for accelerated chronic wound healing.* Materials Science and Engineering: C, 2017. **72**: p. 394-404.
66. Paladini, F. and M. Pollini, *Antimicrobial Silver Nanoparticles for Wound Healing Application: Progress and Future Trends.* Materials (Basel), 2019. **12**(16).
67. Kwan, K.H.L., et al., *Modulation of collagen alignment by silver nanoparticles results in better mechanical properties in wound healing.* Nanomedicine: Nanotechnology, Biology and Medicine, 2011. **7**(4): p. 497-504.
68. Fang, R.C. and R.D. Galiano, *A review of becaplermin gel in the treatment of diabetic neuropathic foot ulcers.* Biologics: targets & therapy 2008. **2**(1): p. 1.
69. Papanas, N. and E. Maltezos, *Becaplermin gel in the treatment of diabetic neuropathic foot ulcers.* Clin Interv Aging, 2008. **3**(2): p. 233-40.
70. Roukis, T.S., T. Zgonis, and B. Tiernan, *Autologous platelet-rich plasma for wound and osseous healing: A review of the literature and commercially available products.* Advances in Therapy, 2006. **23**(2): p. 218-237.
71. Lacci, K.M. and A. Dardik, *Platelet-rich plasma: support for its use in wound healing.* The Yale journal of biology and medicine, 2010. **83**(1): p. 1-9.

72. Petrova, N. and M. Edmonds, *Emerging drugs for diabetic foot ulcers.* Expert Opin Emerg Drugs, 2006. **11**(4): p. 709-724.
73. Abdelkader, D.H., et al., *Enhanced cutaneous wound healing in rats following topical delivery of insulin-loaded nanoparticles embedded in poly(vinyl alcohol)-borate hydrogels.* Drug Delivery and Translational Research, 2018. **8**(5): p. 1053-1065.
74. Pardeike, J., A. Hommoss, and R.H. Müller, *Lipid nanoparticles (SLN, NLC) in cosmetic and pharmaceutical dermal products.* International Journal of Pharmaceutics, 2009. **366**(1): p. 170-184.
75. Prausnitz, M.R., *A peptide chaperone for transdermal drug delivery.* Nature Biotechnology 2006. **24**(4): p. 416-7.
76. Kaplani, K., et al., *Wound healing related agents: Ongoing research and perspectives.* Advanced Drug Delivery Reviews, 2018. **129**: p. 242-253.
77. El Maghraby, G.M., B.W. Barry, and A.C. Williams, *Liposomes and skin: From drug delivery to model membranes.* European Journal of Pharmaceutical Sciences, 2008. **34**(4): p. 203-222.
78. Ferreira, H., et al., *Functionalization of gauzes with liposomes entrapping an anti-inflammatory drug: A strategy to improve wound healing.* Reactive and Functional Polymers, 2013. **73**(10): p. 1328-1334.
79. Dawoud, M.H., et al., *Response surface optimization and in-vitro evaluation of sustained release topical insulin liposomal spray for wound healing.* Journal of Applied Pharmaceutical Science, 2018(8): p. 22-29.
80. Dawoud, M.H.S., et al., *Insulin mucoadhesive liposomal gel for wound healing: a formulation with sustained release and extended stability using quality by design approach.* AAPS PharmSciTech, 2019. **20**(4): p. 158.
81. Puglia, C. and F. Bonina, *Lipid nanoparticles as novel delivery systems for cosmetics and dermal pharmaceuticals.* Expert Opinion on Drug Delivery, 2012. **9**(4): p. 429-441.
82. Gainza, G., et al., *A novel strategy for the treatment of chronic wounds based on the topical administration of rhEGF-loaded lipid nanoparticles: In vitro bioactivity and in vivo effectiveness in healing-impaired db/db mice.* Journal of Controlled Release, 2014. **185**: p. 51-61.
83. Gainza, G., et al., *The topical administration of rhEGF-loaded nanostructured lipid carriers (rhEGF-NLC) improves healing in a porcine full-thickness excisional wound model.* Journal of Controlled Release, 2015. **197**: p. 41-47.
84. Fonte, P., et al., *Polymer-based nanoparticles for oral insulin delivery: Revisited approaches.* Biotechnology advances, 2015. **33**(6 Pt 3): p. 1342-1354.
85. Yang, J., et al., *Construction and characterization of Mesona chinensis polysaccharide-chitosan hydrogels, role of chitosan deacetylation degree.* Carbohydrate Polymers, 2021. **257**.
86. Patrulea, V., et al., *Chitosan as a starting material for wound healing applications.* European Journal of Pharmaceutics and Biopharmaceutics, 2015. **97**: p. 417-426.
87. Ahmed, S. and S. Ikram, *Chitosan based scaffolds and their applications in wound healing.* Achievements in the Life Sciences, 2016. **10**(1): p. 27-37.
88. Ehterami, A., et al., *In vitro and in vivo study of PCL/COLL wound dressing loaded with insulin-chitosan nanoparticles on cutaneous wound healing in rats model.* International Journal of Biological Macromolecules, 2018. **117**: p. 601-609.
89. Mohammed, M.A., et al., *An Overview of Chitosan Nanoparticles and Its Application in Non-Parenteral Drug Delivery.* Pharmaceutics 2017. **9**(4): p. 53.
90. Aderibigbe, B.A. and B. Buyana, *Alginate in wound dressings.* Pharmaceutics, 2018. **10**(2).
91. Borselli, C., et al., *Functional muscle regeneration with combined delivery of angiogenesis and myogenesis factors.* 2010. **107**(8): p. 3287-3292.
92. Litwiniuk, M., et al., *Hyaluronic acid in inflammation and tissue regeneration.* Wounds 2016. **28**(3): p. 78-88.
93. Kavasi, R.-M., et al., *HA metabolism in skin homeostasis and inflammatory disease.* Food and Chemical Toxicology, 2017. **101**: p. 128-138.

94. Hirakura, T., et al., *Hybrid hyaluronan hydrogel encapsulating nanogel as a protein nanocarrier: New system for sustained delivery of protein with a chaperone-like function.* Journal of Controlled Release, 2010. **142**(3): p. 483-489.
95. Fonte, P., et al., *Annealing as a tool for the optimization of lyophilization and ensuring of the stability of protein-loaded PLGA nanoparticles.* International Journal of Pharmaceutics, 2016. **503**(1-2): p. 163-173.
96. Fonte, P., et al., *Annealing as a tool for the optimization of lyophilization and ensuring of the stability of protein-loaded PLGA nanoparticles.* International Journal of Pharmaceutics, 2016. **503**(1): p. 163-173.
97. Fonte, P., et al., *Effect of the freezing step in the stability and bioactivity of protein-loaded PLGA nanoparticles upon lyophilization.* Pharmaceutical Research, 2016. **33**(11): p. 2777-2793.
98. Ulery, B.D., L.S. Nair, and C.T. Laurencin, *Biomedical applications of biodegradable polymers.* Journal of Polymer Science Part B: Polymer Physics, 2011. **49**(12): p. 832-864.
99. Hrynyk, M., et al., *Alginate-PEG Sponge Architecture and Role in the Design of Insulin Release Dressings.* Biomacromolecules, 2012. **13**(5): p. 1478-1485.
100. Abdelkader, D.H., et al., *Effect of poly(ethylene glycol) on insulin stability and cutaneous cell proliferation in vitro following cytoplasmic delivery of insulin-loaded nanoparticulate carriers – A potential topical wound management approach.* European Journal of Pharmaceutical Sciences, 2018. **114**: p. 372-384.
101. Solaro, R., A. Corti, and E. Chiellini, *Biodegradation of poly (vinyl alcohol) with different molecular weights and degree of hydrolysis.* Polymers for Advanced Technologies, 2000. **11**(8-12): p. 873-878.
102. Mohseni, M., et al., *A comparative study of wound dressings loaded with silver sulfadiazine and silver nanoparticles: In vitro and in vivo evaluation.* International Journal of Pharmaceutics, 2019. **564**: p. 350-358.
103. Casimiro, M.H., et al., *Chitosan-based matrices prepared by gamma irradiation for tissue regeneration: Structural properties vs. Preparation method.* Topics in Current Chemistry, 2016. **375**(1): p. 5.
104. Li, Z., et al., *Fabrication of PVA/PAAm IPN hydrogel with high adhesion and enhanced mechanical properties for body sensors and antibacterial activity.* European Polymer Journal, 2021. **146**: p. 110253.
105. Zhang, C., et al., *High-Performance Photopolymerized Poly(vinyl alcohol)/Silica Nanocomposite Hydrogels with Enhanced Cell Adhesion.* ACS Applied Materials & Interfaces, 2018. **10**(33): p. 27692-27700.
106. Zhang, S., et al., *One-Step Preparation of a Highly Stretchable, Conductive, and Transparent Poly(vinyl alcohol)–Phytic Acid Hydrogel for Casual Writing Circuits.* ACS Applied Materials & Interfaces, 2019. **11**(35): p. 32441-32448.
107. Bolto, B., et al., *Crosslinked poly (vinyl alcohol) membranes.* Progress in polymer science 2009. **34**(9): p. 969-981.
108. Tamariz, E. and A. Rios-Ramírez, *Biodegradation of medical purpose polymeric materials and their impact on biocompatibility.* Biodegradation-Life of Science Croatia: Intech, 2013: p. 1-29.
109. Mody, V.V., et al., *Introduction to metallic nanoparticles.* Journal of Pharmacy Bioallied Sciences, 2010. **2**(4): p. 282.
110. Rai, M., A. Yadav, and A. Gade, *Silver nanoparticles as a new generation of antimicrobials.* Biotechnology Advances, 2009. **27**(1): p. 76-83.
111. Liu, X., et al., *Silver nanoparticles mediate differential responses in keratinocytes and fibroblasts during skin wound healing.* ChemMedChem, 2010. **5**(3): p. 468-475.
112. Mebert, A.M., et al., *Nanoengineered silica: Properties, applications and toxicity.* Food and Chemical Toxicology, 2017. **109**: p. 753-770.

113. Ponnanikajamideen, M., et al., *In vivo type 2 diabetes and wound-healing effects of antioxidant gold nanoparticles synthesized using the insulin plant Chamaecostus cuspidatus in albino rats.* Canadian journal of diabetes, 2019. **43**(2): p. 82-89.
114. Priddy-Arrington, T.R., et al., *Proactive biomaterials for chronic wound management and treatment.* Current Opinion in Biomedical Engineering, 2021. **20**: p. 100327.
115. Singh, T.R.R., G. Laverty, and R. Donnelly, *Hydrogels: design, synthesis and application in drug delivery and regenerative medicine*. 2018: CRC Press.
116. Utech, S. and A.R. Boccaccini, *A review of hydrogel-based composites for biomedical applications: enhancement of hydrogel properties by addition of rigid inorganic fillers.* Journal of materials science, 2016. **51**(1): p. 271-310.
117. Kamoun, E.A., E.-R.S. Kenawy, and X. Chen, *A review on polymeric hydrogel membranes for wound dressing applications: PVA-based hydrogel dressings.* Journal of advanced research 2017. **8**(3): p. 217-233.
118. Ding, M., et al., *Multifunctional soft machines based on stimuli-responsive hydrogels: from freestanding hydrogels to smart integrated systems.* Materials Today Advances 2020. **8**: p. 100088.
119. Shamloo, A., et al., *Fabrication and evaluation of chitosan/gelatin/PVA hydrogel incorporating honey for wound healing applications: An in vitro, in vivo study.* International Journal of Pharmaceutics, 2021. **592**: p. 120068.
120. Choe, G., et al., *Hydrogel Biomaterials for Stem Cell Microencapsulation.* Polymers, 2018. **10**(9):997.
121. Yuan, Y., S. Shen, and D. Fan, *A physicochemical double cross-linked multifunctional hydrogel for dynamic burn wound healing: shape adaptability, injectable self-healing property and enhanced adhesion.* Biomaterials, 2021: p. 120838.
122. Jeske, R., et al., *Agitation in a microcarrier-based spinner flask bioreactor modulates homeostasis of human mesenchymal stem cells.* Biochemical Engineering Journal, 2021. **168**: p. 107947.
123. Mora-Boza, A., et al., *Microfluidics generation of chitosan microgels containing glycerylphytate crosslinker for in situ human mesenchymal stem cells encapsulation.* Materials Science and Engineering: C, 2021. **120**: p. 111716.
124. Bashir, N.Z., *The role of insulin-like growth factors in modulating the activity of dental mesenchymal stem cells.* Archives of Oral Biology, 2021. **122**: p. 104993.
125. Gilevich, I.V., et al., *Effects of growth Factors on mobilization of mesenchymal stem cells.* Bulletin of Experimental Biology and Medicine, 2017. **162**: p. 684-686.
126. Nie, W.B., D. Zhang, and L.S. Wang, *Growth factor gene-modified mesenchymal stem cells in tissue regeneration.* Drug Design, Development and Therapy, 2020. **14**: p. 1241-1256.
127. Sharma, P., et al., *Stem cells and growth factors-based delivery approaches for chronic wound repair and regeneration: A promise to heal from within.* Life Sciences, 2021: p. 118932.
128. Kim, J.W., et al., *The effects of topical mesenchymal stem cell transplantation in canine experimental cutaneous wounds.* Veterinary dermatology, 2013. **24**(2): p. 242-253.
129. Javazon, E.H., et al., *Enhanced epithelial gap closure and increased angiogenesis in wounds of diabetic mice treated with adult murine bone marrow stromal progenitor cells.* Wound Repair and Regeneration 2007. **15**(3): p. 350-359.
130. Kuo, Y.-R., et al., *Bone marrow–derived mesenchymal stem cells enhanced diabetic wound healing through recruitment of tissue regeneration in a rat model of streptozotocin-induced diabetes.* Plastic and reconstructive surgery, 2011. **128**(4): p. 872-880.
131. Ferreira, J.R., et al., *Mesenchymal stromal cell secretome: influencing therapeutic potential by cellular pre-conditioning.* Frontiers in immunology, 2018; **9**: p. 2837.
132. Matsui, F., et al., *Mesenchymal stem cells protect against obstruction-induced renal fibrosis by decreasing STAT3 activation and STAT3-dependent MMP-9 production.* American Journal of Physiology-Renal Physiology, 2017. **312**(1): p. F25-F32.

133. Cappuzzello, C., et al., *Mesenchymal Stromal Cell-Derived PTX3 Promotes Wound Healing via Fibrin Remodeling.* Journal of Investigative Dermatology, 2016. **136**(1): p. 293-300.
134. Li, M., et al., *Mesenchymal stem cell–conditioned medium improves the proliferation and migration of keratinocytes in a diabetes-like microenvironment.* The international journal of lower extremity wounds, 2015. **14**(1): p. 73-86.
135. Saheli, M., et al., *Human mesenchymal stem cells-conditioned medium improves diabetic wound healing mainly through modulating fibroblast behaviors.* Archives of dermatological research, 2020. **312**(5): p. 325-336.
136. Liubaviciute, A., T. Ivaskiene, and G. Biziuleviciene, *Modulated mesenchymal stromal cells improve skin wound healing.* Biologicals, 2020. **67**: p. 1-8.
137. Chen, R., Z. Sun, and D. Chen, *Chapter 11 - Droplet-based microfluidics for cell encapsulation and delivery*, in *Microfluidics for Pharmaceutical Applications*, H.A. Santos, D. Liu, and H. Zhang, Editors. 2019, William Andrew Publishing. p. 307-335.
138. Mesquita, C.R.S., et al., *Continuous-mode encapsulation of human stem cell spheroids using droplet-based glass-capillary microfluidic device for 3D bioprinting technology.* Biochemical Engineering Journal, 2021. **174**: p. 108122.
139. Rakszewska, A., et al., *One drop at a time: toward droplet microfluidics as a versatile tool for single-cell analysis.* NPG Asia Materials, 2014. **6**(10): p. e133-e133.
140. Gupta, A., S.M.S. Murshed, and R. Kumar, *Droplet formation and stability of flows in a microfluidic T-junction.* Applied physics letters, 2009. **94**(16): p. 164107.
141. Gupta, A. and R. Kumar, *Flow regime transition at high capillary numbers in a microfluidic T-junction: Viscosity contrast and geometry effect.* 2010. **22**(12): p. 122001.
142. He, P., D. Barthes-Biesel, and E. Leclerc, *Flow of two immiscible liquids with low viscosity in Y shaped microfluidic systems: effect of geometry.* Microfluidics and nanofluidics, 2010. **9**(2-3): p. 293-301.
143. Mazutis, L., et al., *Single-cell analysis and sorting using droplet-based microfluidics.* Nature Protocols, 2013. **8**(5): p. 870-891.
144. Brouzes, E., et al., *Droplet microfluidic technology for single-cell high-throughput screening.* Proceedings of the National Academy of Sciences, 2009. **106**(34): p. 14195-14200.
145. Zhu, P. and L. Wang, *Passive and active droplet generation with microfluidics: a review.* Lab Chip, 2016. **17**: p. 34-75.
146. Garstecki, P., et al., *Formation of droplets and bubbles in a microfluidic T-junction—scaling and mechanism of break-up.* Lab on a Chip, 2006. **6**(3): p. 437-446.
147. Yao, J., et al., *The Effect of Oil Viscosity on Droplet Generation Rate and Droplet Size in a T-Junction Microfluidic Droplet Generator.* Micromachines, 2019. **10**(12): p. 808.
148. Kim, S.J., et al., *Engineering multi-cellular spheroids for tissue engineering and regenerative medicine.* Advanced Healthcare Materials, 2020. **9**(23).
149. An, C., et al., *Continuous microfluidic encapsulation of single mesenchymal stem cells using alginate microgels as injectable fillers for bone regeneration.* Acta Biomaterialia, 2020. **111**: p. 181-196.
150. Zhang, R., et al., *Alginate/laponite hydrogel microspheres co-encapsulating dental pulp stem cells and VEGF for endodontic regeneration.* Acta Biomaterialia, 2020. **113**: p. 305-316.
151. Gainza, G., et al., *Advances in drug delivery systems (DDSs) to release growth factors for wound healing and skin regeneration.* Nanomedicine, 2015. **11**(6): p. 1551-1573.
152. Li, B., et al., *Past, present, and future of microcarrier-based tissue engineering.* Journal of Orthopaedic Translation, 2015. **3**(2): p. 51-57.
153. Krausz, A.E., et al., *Curcumin-encapsulated nanoparticles as innovative antimicrobial and wound healing agent.* Nanomedicine : nanotechnology, biology, and medicine, 2015. **11**(1): p. 195-206.
154. Ye, Q., N. Georges, and C. Selomulya, *Microencapsulation of active ingredients in functional foods: From research stage to commercial food products.* Trends in Food Science and Technology, 2018. **78**: p. 167-179.

155. Fathi, M., M.R. Mozafari, and M. Mohebbi, *Nanoencapsulation of food ingredients using lipid based delivery systems.* Trends in Food Science and Technology, 2012. **23**(1): p. 13-27.
156. de Souza Simões, L., et al., *Micro- and nano bio-based delivery systems for food applications: In vitro behavior.* Advances in Colloid and Interface Science, 2017. **243**: p. 23-45.
157. Fonte, P., et al., *Effect of cryoprotectants on the porosity and stability of insulin-loaded PLGA nanoparticles after freeze-drying.* Biomatter, 2012. **2**(4): p. 329-339.
158. Loughlin, R.G., et al., *Modulation of gel formation and drug-release characteristics of lidocaine-loaded poly(vinyl alcohol)-tetraborate hydrogel systems using scavenger polyol sugars.* European Journal of Pharmaceutics and Biopharmaceutics, 2008. **69**(3): p. 1135-1146.
159. Spoljaric, S., et al., *Stable, self-healing hydrogels from nanofibrillated cellulose, poly(vinyl alcohol) and borax via reversible crosslinking.* European Polymer Journal, 2014. **56**(1): p. 105-117.
160. Lin, H.L., et al., *Complexation equilibrium constants of poly(vinyl alcohol)-borax dilute aqueous solutions - Consideration of electrostatic charge repulsion and free ions charge shielding effect.* Journal of Polymer Research, 2002. **9**(4): p. 233-238.
161. Lopes, M.A., et al., *Probing insulin bioactivity in oral nanoparticles produced by ultrasonication-assisted emulsification/internal gelation.* International journal of nanomedicine, 2015. **10**: p. 5865-5880.
162. Fonte, P., et al., *Chapter fifteen - Chitosan-coated solid lipid nanoparticles for insulin delivery*, in *Methods in Enzymology*, N. Düzgüneş, Editor. 2012, Academic Press. p. 295-314.
163. Kelly, S.M., T.J. Jess, and N.C. Price, *How to study proteins by circular dichroism.* Biochimica et Biophysica Acta (BBA) - Proteins and Proteomics, 2005. **1751**(2): p. 119-139.
164. Ahmad, A., et al., *Early Events in the Fibrillation of Monomeric Insulin*.* Journal of Biological Chemistry, 2005. **280**(52): p. 42669-42675.
165. Maskevich, A.A., et al., *Spectral properties of thioflavin T in solvents with different dielectric properties and in a fibril-incorporated form.* Journal of Proteome Research, 2007. **6**(4): p. 1392-1401.
166. Fonte, P., et al., *Stability study perspective of the effect of freeze-drying using cryoprotectants on the structure of insulin loaded into PLGA nanoparticles.* Biomacromolecules, 2014. **15**(10): p. 3753-3765.